Research Square

Preprints are preliminary reports that have not undergone peer review.
They should not be considered conclusive, used to inform clinical practice,
or referenced by the media as validated information.

Secretion Inhibition of CCL2 by Decorin in colorectal cancer tumor-associated macrophages and the synergistic therapeutic effect with PD-1inhibitor

Xiuli Bi

xiulibi@lnu.edu.cn

Liaoning University

Xianda Cheng

Liaoning University

Xiaoqin Luo

Liaoning University

Yue Liu

Liaoning University

Ziqi Fang

Wenzhou Institute

Lili Chen

Liaoning University

Chen Zhang

Liaoning University

Jin Wang

Liaoning University

Zhe Yang

Liaoning University

Min Wu

University of Chinese Academy of Sciences https://orcid.org/0000-0003-1205-982X

Article

Keywords: Decorin, CCL2, JAK2-STAT3, tumor-associated macrophages, colorectal cancer

Posted Date: June 15th, 2026

DOI: https://doi.org/10.21203/rs.3.rs-9679851/v1

License: This work is licensed under a Creative Commons Attribution 4.0 International License.
Read Full License

Additional Declarations: (Not answered)

Secretion Inhibition of CCL2 by Decorin in colorectal cancer tumor-associated macrophages and the synergistic therapeutic effect with PD-1inhibitor

Xianda Cheng[a, c] ,Xiaoqin Luo[a] ,Yue Liu[a] Ziqi Fang[b,c], Lili Chen[a], Chen Zhang[a], Jin Wang[a], Zhe Yang[a], Min Wu[c]*, Xiuli Bi[a]*

[a]College of Life Science, Liaoning University, Shenyang, 110036, China;

[b]School of Medical Information Engineering, Gannan Medical University, Ganzhou 341000, China;

[c]Wenzhou Institute, University of Chinese Academy of Sciences, Wenzhou 325000, China;

*Corresponding authors:

E-mail address:

minwoo2022@126.com (Min Wu)

xiulibi@lnu.edu.cn; xiulibi@gmail.com (Xiuli Bi)

Abstract

The mechanisms of occurrence and development of colorectal cancer (CRC) are highly complex and multifaceted, in which tumor-associated macrophages (TAMs) play a key role, and their changes in function and phenotype have a significant impact on tumor progression. The dysregulated expression of decorin (DCN) in colorectal cancer promotes the occurrence and development of colorectal cancer has been reported previously, but its specific mechanism in regulating TAMs and thus affecting the progression of colorectal cancer remains to be fully unfolded. In this study, CCL2 expression in myeloid cells was upregulated in the colon tissue of DCN-deficient mice was revealed through single-cell RNA sequencing analysis, and it was speculated that there might be a potential regulatory relationship between these two factors. Meanwhile, DCN expression down-regulated and CCL2 specifically highly expressed in M2 TAMs in the CRC tumor microenvironment was found by using TIMER, TISIDB and GEPIA online databases analysis. Mining of the single-cell sequencing results revealed that JAK2-STAT3 might involve in the secretion inhibition of CCL2 by DCN in macrophages. Further, ELISA, immunofluorescence and WB results in vitro confirmed that DCN could inhibit the secretion of CCL2 in TAMs by inhibiting JAK2-STAT3, and subsequently inhibiting the migration of macrophages mediated by CCL2. Immunoprecipitation mass spectrometry and immunoprecipitation experiments determined that DCN could directly act on TLR2 on the membrane surface of TAMs, which might serve as a key factor for DCN regulation on JAK2-STAT3 and eventually leads to inhibit the secretion of CCL2. Finally, TAMs overexpressing DCN can inhibit the polarization of M2 TAMs and their mediated immune escape can be combined with PD-1 immune checkpoint inhibitors(PD-1-IN-17) to

inhibit the development of colorectal cancer were found in vivo experiments. In summary, our study revealed the specific mechanism by which DCN inhibited the secretion of CCL2 in TAMs in CRC, indicating a potential strategy for targeted and combined immunotherapy of CRC patients.

Keywords: Decorin; CCL2; JAK2-STAT3; tumor-associated macrophages; colorectal cancer

Introduction

As a highly prevalent gastrointestinal malignancy globally, the prevention and treatment of colorectal cancer have become a central issue in the field of public health. According to the American Association for Cancer Research (AACR) Cancer Progress Report 2025, colorectal cancer ranks third in global cancer incidence and second in mortality; in 2025, the number of new colorectal cancer cases worldwide is projected to exceed 1.2 million, with approximately 700,000 deaths[1]. Traditional treatment approaches primarily rely on surgery, chemotherapy, radiotherapy, and targeted therapies against specific molecular targets (such as EGFR and VEGF)[2]. Although these therapies have improved patient prognosis to some extent, the five-year survival rate for patients with advanced or metastatic CRC (mCRC) remains unsatisfactory, highlighting the urgent need for more effective treatment strategies[3].

Over the past decade, tumor immunotherapy, particularly the advent of immune checkpoint inhibitors (ICIs) represented by programmed death receptor-1 (PD-1) and its ligand (PD-L1)[4], has brought revolutionary breakthroughs in the treatment of various malignant tumors[4,5]. However, in the field of colorectal cancer (CRC), the therapeutic effect of immunotherapy is relatively limited[6]. The main reason for this is the presence of a large number of immunosuppressive tumor-infiltrating immune cells in the microenvironment of some colorectal cancers, creating an "immune-excluded" microenvironment that makes it difficult for immune cells to perform their normal immune functions[6,7]. In addition, the spatial heterogeneity of the colorectal cancer immune microenvironment is also one of the reasons for the limited effectiveness of immunotherapy[8]. The variability of anti-tumor immune responses is not only closely related to disease progression but also directly affects the

response to treatment regimens[9,10]. In the evolution of immune heterogeneity in the tumor microenvironment, the abnormal accumulation of M2 tumor-infiltrating macrophages is one of the important reasons why immunotherapy is difficult to activate the immune response of tumor-infiltrating immune cells[11,12]. These tumor-infiltrating macrophages secrete inhibitory factors such as IL-10 and TGF-β, and highly express markers such as CD163 and CD206, forming an immunosuppressive microenvironment, promoting tumor angiogenesis, invasion and metastasis, and inhibiting tumor cell apoptosis[13]. They also inhibit the activation of antigen presentation pathways, making it difficult for immune cells to perform normal immune killing functions, thereby inducing tumor cells to evade immune surveillance[14]. Currently, targeted therapy against M2 TAMs is one of the important strategies for improving the effectiveness of immunotherapy in colorectal cancer. Current research has shown that targeting the MAPK and STAT signaling pathways in macrophages significantly promotes the repolarization of M2 TAMs and enhances the effectiveness of PD-1 immunotherapy[15,16].

CCL2, as a member of the chemokine family, not only induces the directional migration of macrophages but is also a key factor in inducing the M2 polarization of M0-type macrophages and activating the PD-1 signaling pathway[17]. The PD-1 resistance of tumor-infiltrating macrophages induced by CCL2 is a significant reason why anti-PD-1 immunotherapy is ineffective in certain types of colorectal cancer and esophageal cancer[18]. Targeting the expression of CCL2 in M2-type tumor-associated macrophages (TAMs) during tumor development is also an important strategy in cancer immunotherapy, and combined treatment with immune checkpoint inhibitors has achieved significant results in various cancers, including gastric cancer and lung cancer[19,20].

Studies have shown that decorin is an effective broad-spectrum anti-cancer tumor suppressor, with low expression levels in most cancers[21,22]. Decorin interacts with receptor tyrosine kinases and acts as a broad-spectrum receptor tyrosine kinase inhibitor, thereby inhibiting oncogenic signaling[23,24]. Decorin deficiency promotes epithelial-mesenchymal transition and enhances cancer spread and metastasis. DCN can indirectly downregulate the bioactivity of transforming growth factor-β1 (TGF-β1), thereby counteracting the transcriptional repression of PDCD4[25]. Therefore, anti-inflammatory mediators such as IL-10 are translationally repressed by PDCD4, leading to a pro-inflammatory tumor microenvironment. DCN's ability to regulate inflammation is crucial for understanding its role[26] in tumor biology, as a pro-inflammatory tumor microenvironment can hinder tumor growth[27]. Although DCN can induce pro-inflammatory responses, it has also been reported that the DCN core protein downregulates chemotactic and inflammatory genes in leukocytes. Therefore, the role of DCN in regulating inflammation and immune responses appears complex and requires further research to clarify whether DCN elicits a pro-inflammatory or anti-inflammatory response in each specific context. Merline et al. found that DCN can increase the production of TNF-α and IL-12p70[26]. On the other hand, studies by Buraschi et al. indicated that anti-inflammatory gene transcription is inhibited under DCN stimulation[28]. Therefore, it is conceivable that in different in vivo models of fibrotic diseases, animals with DCN knockout exhibit a pro-inflammatory phenotype, while in experimental therapeutic trials, the addition of exogenous DCN can suppress inflammation[29,30].

Materials and Methods

Mouse Breeding and Tissue Sampling

All experimental procedures in this study were approved by the Animal Ethics Committee of Liaoning University. Procedures for animal handling and tissue sampling were conducted in compliance with protocols approved by the Animal Care and Use Committee of Liaoning University. C57BL/6 DCN $^{(+/-)}$ heterozygous mice were obtained from Liaoning University, and newborn mice were obtained by breeding heterozygous mice. The genotypes of the newborn mice were identified, and several homozygous mice were obtained, namely DCN knockout mice. In addition to type mouse DCN $^{(-/-)}$ and wild type mouse DCN $^{(+/+)}$, we also used select healthy wild-type mice with a body weight of about 18-22 g and an age of 6-8 weeks as normal controls. The mice were sacrificed, and the colon tissues were removed for experiments.

Establishment of subcutaneous tumor-bearing model in mice and drug administration strategy

The TAMs-targeting lentiviral vector pGLV-Mrc1-Promoter-Dcn-3xFlag-EF1-copGFP-Puro was constructed by J GeneAdv Co. Ltd. The concentration was $1x10^8$ vg/ml. Bal b/c wild-type mice were purchased from Zhejiang Provincial Animal Center. All experimental procedures in this study were approved by the Animal Ethics Committee of the Wenzhou Institute of the University of Chinese Academy of Sciences. Animal handling and tissue sampling procedures were conducted in strict accordance with the protocols approved by the Animal Ethics and Use Committee of the Wenzhou Institute of the University of Chinese Academy of Sciences. Anti-Mouse PD-1 Antibody (RMP1-14) was purchased from GLPBIO. The injection dose was

10 mg/kg, administered every 72 hours for a total of three injections. Healthy male mice aged 4 weeks and weighing 14-16 g were used for subcutaneous tumor modeling. Each mouse was inoculated with 5×10^6 cells. The calculation formula for mouse solid tumors was π/6×long diameter×short diameter^2. The mice were injected with DCN overexpression lentivirus intratumorally with a subcutaneous tumor volume of about 100 mm3, and the injection was repeated every 72 hours. The mice were killed after three injections (Volume is about 1000mm^3).

Single RNA-seq

Fresh tissue was washed with Hanks balanced salt solution, minced into small pieces, digested with sCelLive Tissue Dissociation Solution (Singleron), filtered through a 40-micron sterile strainer, centrifuged (300×g, 4°C) to remove supernatant, resuspended with PBS/DMEM, then stained with trypan blue to microscopically evaluated cell viability. Single-cell suspensions (2×10^5 cells/mL) were loaded onto a microwell chip using the Singleron Matrix Single Cell Processing System. Barcoding beads were subsequently collected from the microwell chip, followed by reverse transcription of captured mRNA. The obtained cDNA was amplified by PCR, then fragmented and ligated with sequencing adapters. The scRNA-seq libraries were constructed by using the GEXSCOPE Single Cell RNA Library Kits (Singleron). Individual libraries were pooled and sequenced on Illumina novaseq 6000 with 150bp paired end reads.

Online database analysis

TIMER2.0 (http://timer.cistrome.org/) and TISCH (http://cis.hku.hk/TISIDB/) explore the correlation between target genes and tumor-related immune cells, GEPIA2 (http://gepia2.cancer-pku.cn/#index) explores the role of target genes in tumor immunotherapy, and TISCH (tisch.comp-genomics.org/home/) is used to verify single-cell sequencing results.

Cell culture

The following cell lines were mainly used in this study: THP-1 (#CL-0233, Procell), sw480 (#CL-0223, Procell), HCT116 (#CL-0096, Procell), sw620 (#CL-0225, Procell). The cells were cultured in RPMI-1640 (#PM150110, Procell) with 10% foetal bovine serum (#164210, Procell) and 1% penicillin/streptomycin (C0222, Beyotime) at 37°C with 5% CO2.

Western blot

Total protein extraction reagent for cultured cells (Prod: AR0103-100, BOSTER) was used for protein extraction. After the lysis buffer was added, the mixture was incubated on ice for 30 minutes and centrifuged at 10,000 g for 10 minutes to collect the supernatant as the protein sample. For western blotting, the primary antibodies against the following proteins were used: CCL2 (1:1000; #ab214819,Abcam), p-JAK2 (1:1000; #32101, Abcam), JAK2 (1:1000; #ab108596, Abcam), STAT3 (1:1000; #68153, Abcam), DCN (1:1000; #175404, Abcam), CCR2 (1:1000; #12199, Cell Signaling Technology), TLR2 (1:1000; #12276, Cell Signaling Technology), GAPDH (1:2000; #WAB45855, Bio-swamp). The secondary antibodies against the following proteins were used: HRP-conjugated Goat Anti-Rabbit IgG(H+L) (1:2000;

#SA00001-2, Proteintech), HRP-conjugated Goat Anti-Mouse IgG(H+L) (1:2000; #SA00001-1, Proteintech). Equal amounts of proteins from different groups were resolved via 10% or 12% SDS–PAGE and then transferred onto NC membranes (Sangon Biotech, F619511-0005). Subsequently, the membranes were blocked for 2 h at RT with 5% milk in TBST and then incubated overnight at 4°C with primary antibodies (Table S3). Then, the membranes were washed three times with TBST and incubated with horseradish peroxidase-conjugated anti-rabbit or anti-mouse IgG antibodies at temperature for 1 h. The target protein bands were visualized using an enhanced chemiluminescence high-sensitivity reagent (MA0186, Meilunbio) and a ChemiDoc Imager (Micro Chemi). The densitometric values were determined using the ImageJ software (National Institutes of Health, USA). The relative protein levels were normalized against the levels of β-actin/GAPDH, used as an internal control.

RNA extraction and quantitative reverse transcriptase-polymerase chain reaction (RT-qPCR) analysis:

RNAprep Pure Total RNA Extraction Kit for Cultured Cells/Bacteria (DP430, TIANGEN) was used for cell RNA extraction. HiScript II Q RT SuperMix for qPCR (+gDNA wiper) (Cat: R223-01, Vazyme) was used for RNA reverse transcription. qPCR mix was purchased from Novozymes Biopharmaceuticals (Cat: Q712-02, Vazyme), and the qPCR conditions were 95°C, 15 sec, 95°C, 10 sec, 60°C, 30 sec, and 40 cycles. The design of primers for related genes is shown in the supplementary materials.

Transwell in vitro co-culture:

Matrigel was purchased from Corning (#354248), and transwell co-culture chamber was purchased from Merck (#CLS3378), and co-culture was performed for 48 h.

Lentivirus and siRNA transfection:

The lentiviral vector pCDH-CMV-EF1A-GFP-T2A-puro was selected as the DCN overexpression vector, and the lentiviral coating was completed by J GeneAdv Co. Ltd. The concentration was $1x10^8$ μg/ml. The cells were resuspended in serum-free medium and incubated with lentiviral solution at 37°C for 30 minutes, then resuspended in a complete medium and transferred to a six-well plate for 12 hours, and then replaced with complete medium for 48 hours to complete lentiviral transfection. For siRNA transfection, the siRNA dry powder was dissolved in DEPC water and mixed with the transfection reagent, and added to the six-well plate with cells after continuous pipetting for more than 20 times. The gene interference effect can be observed 24 hours after transfection. The TLR2-siRNA sequence and the DCN overexpression vector sequence are both listed in the supplementary materials.

Co-immunoprecipitation mass spectrometry analysis and immunoprecipitation-mass spectrometry analysis:

The immunoprecipitation kit was purchased from Thermo Fisher Scientific (#88805), and the experimental steps were consistent with the kit instructions. since the applied DCN antibody is not available for Co-IP assay, we established FLAG-tagged plasmids to pull down the complex that interacts with DCN. The DYKDDDDK tag polyclonal antibody (Binds to flag; 5ug; #20543-1-AP, Proteintech) is used to bind to magnetic beads. For MS, The collected protein

was sent to GeneAdv Co. Ltd, (Suzhou, China) for MS analysis.

TAMs sorting and flow cytometry

In a 100 mm cell culture dish, the tumor tissue was cut into 0.1 mm^3 pieces with scissors, added to a culture medium containing type IV collagenase (1 mg/ml, BS165, Biosharp), hyaluronidase (0.2 mg/ml, 37326-33-3, Merk) and DNAse I (0.2 mg/ml,10104159001,Roche), and digested at 37°C for 2 hours. The cell suspension was collected and sieved through a 40 um cell sieve to remove connective tissue fragments. The cells were centrifuged at 800 g for 5 minutes, and the cell suspension and percoll were slowly added to a centrifuge tube at a volume ratio of 2:1. The tube was centrifuged at 20°C for 20 minutes. After culturing in 1640 complete culture medium for 48 hours, the purity of TAMs was analyzed by flow cytometry. The single tumor cell suspension was stained in the dark with anti-CD11b-bv421 and anti-CD205-FITC for 30 minutes, and the situation of TAMs in the tumor was evaluated by flow cytometry (CytoFLEX LX, Beckman).

Immunofluorescence:

The cells were fixed with 4% paraformaldehyde for 20 minutes, blocked with 1% BSA for 1 hour, washed with PBS three times, incubated with primary antibody overnight, equilibrated to room temperature, incubated with fluorescent secondary antibody for one hour, and stained with DAPI for 15 minutes. The following fluorescent secondary antibodies were used: Goat anti-rat IgG H&L (Alexa Fluor® 488) (1:100; #ab150165, Abcam), goat anti-rabbit IgG H&L (Alexa Fluor® 488) (1:100; #ab150077, Abcam), goat anti-mouse IgG H&L (Alexa Fluor® 594)

(1:100; #ab150116, Abcam). Fluorescence imaging was taken using confocal microscopy (Nikon LSM 980).

Enzyme-linked immunosorbent assay (ELISA):

Serum levels of CCL2 were measured by commercial ELISA kits (#JL19344-96T for CCL2, JONLNBIO). A total of 100 μL serum was placed into a 96-well plate coated with an Ab specific to the marker and incubated at 37℃ for 60 min. Then, the diluted biotin-conjugated Ab (100 μL) was added to the wells and incubated at 37℃ for 60 min. Subsequently, Avidin-HRP conjugate (100 μL) was supplemented into the wells at 37℃ for 30 min, then washed before reaction with 3,3',5,5'-tetramethylbenzidine (90 μL) as the chromogenic reagent occurred in the dark for 10-20 min. The reaction was terminated with a sulfuric acid solution (60 μL) and the absorbance was measured using EnSight Multimode Plate Reader (Perkin Elmer, Boston,MA, USA) at 450 nm.

Protein molecular docking：

The X-ray crystal structures of TLR2 (6NIG) were retrieved from the Protein Data Bank. The predicted structures of PGS2 were generated by Alphafold. To ensure the accuracy of the docking results, the protein was prepared by the AutoDockTools-1.5.7, and the water molecules were manually eliminated from the protein and the polar hydrogen was added. Docking Web Server (GRAMM) was used for protein-protein docking. The resulting protein-protein complex was also manually optimized by removing water and adding polar hydrogen by the AutoDockTools-1.5.7. Finally, the protein-protein interactions were predicted and the

protein-protein interaction figure was generated by PyMOL.

Molecular dynamics analysis

The molecular dynamics simulations were carried out with Desmond/Maestro noncommercial version 2022.1 as a molecular dynamic's software. TIP3P water molecules were added to the systems, which were then neutralized by 0.15 M NaCl solution. After minimization and relaxation of the system, the production simulation was performed for 100 ns in an isothermal-isobaric ensemble at 300 K and 1 bar. Trajectory coordinates were recorded every 100 ps. The molecular dynamics analysis was performed using Simulation Interaction Diagram from Desmond.

Paraffin sides experiment and HE staining experiment

Fresh tissue is immediately put into tissue fixative or a special fixative corresponding to the tissue for more than 24 hours, put the dehydration box into the dehydrator in order to dehydrate with gradient alcohol. 75% alcohol for 4 hours,85% alcohol for 2 hours,90%alcohol for 2 hours,95% alcohol for 1 hour,anhydrous ethanol I for 30 min,anhydrous ethanol II for 30 min, alcohol benzene for 5~10 min,xylene II for 5~10 min,65℃ melting paraffin I for 1h,65 meltingparaffin II for 1h,65℃ melting paraffin III for 1 hour. Put the trimmed wax block into a paraffin slicer for slicing, with a thickness of 4 μM. The tissue is flattened when the slice floats on the 40 ℃ warm water of the spreading machine, and the tissue is picked up by the glass slides and baked in the oven at 60 ℃. The sections were treated with HD constant staining pretreatment solution for 1 min. Put sections into Hematoxylin solution for 3-5 min, rinse with

tapwater. Then treat the section with Hematoxylin Differentiation solution, rinse with tap water. Treat the section with Hematoxylin Bluing solution, rinse with tap water. Put the sections into absolute ethanol I for 2min-absolute ethanol II for 2min-absolute ethanol III for 2min-normal butanol I for 2min - normal butanol II for 2min-xylene Ⅰ for 2min-xylene Ⅱ for 2min, sealing with neutral gum.

Immunohistochemistry

4% paraformaldehyde -embedded samples were serially sectioned at 4 μm thickness. Antigen retrieval was performed by a pressure cooker for 30 min in 0.01 M citrate buffer (pH 6.0),followed by treatment with 3% hydrogen peroxide for 5 min. Specimens were incubated with monoclonal antibodies against Mouse CD206 (1:500; Abcam), CCL2 (1:500;Abcam), IL-10(1:500;Abcam), TGF-β(1:500;Abcam), PD-1(1:500;Abcam), Ki67(1:500;Abcam), P27(1:500;Abcam), MLH1(1:500;Abcam), overnight at 4 degree. Immunostaining was performed using DAB according to the manufacturer's instructions. For negative control, isotype-matched antibodies were applied. Cells stained with indicated antibody were calculated calculated per field of view, with at least 10 view-fields per section were evaluated at 400× magnification.

Statistical analysis:

The data were expressed as mean ± SEM. The unpaired two tailed Student's t-test was used to compare differences between two groups. Multiple comparisons were performed with one-way ANOVA using Dunnett's multiple comparisons test. Statistical analysis was conducted

using GraphPad Prism (Version 8.0). P < 0.05 was considered statistically significant for all the two-sided tests. In the chart, *represents P<0.05, ** represents P<0.01, and *** represents P<0.001.

Results

Single-cell sequencing results showed upregulation of CCL2 expression in myeloid cells of DCN knockout mice

To investigate the potential role of DCN in colorectal cancer development, we conducted scRNA-seq on colon samples from both wild-type (WT) and DCN knockout homozygotes (HOM) mice. The classification of cell types and their corresponding identification markers are detailed in Supplementary Table 1. Notably, the myeloid cell population primarily consisted of macrophages, with a minor presence of dendritic cells, and the cell types observed in both groups were largely consistent (Fig 1A). Analysis of the clustering results revealed a reduction in the proportion of colon and epithelial cells in the DCN knockout group, accompanied by an increase in immune-related cell types, such as plasma cells and myeloid cells. (Fig 1A).

To determine the polarization type of macrophages accumulated in the colonic tissue of mice after DCN knockout, we investigated the changes in transcriptional levels of markers for different polarization types of intestinal macrophages in two groups of mice. We found that the M2 macrophage marker was upregulated in the macrophage population of the HOM group after DCN knockout. (Fig 1B). We examined the intercellular interactions between the HOM group and the WT group, which show that following the knockout of DCN, there was an increase in intercellular interactions between myeloid cells and other cell types, with the

exception of plasma cells(Fig 1C).

We performed a cytokine interaction analysis on these two cell types, selecting cytokines with elevated expression levels for comparative purposes (Fig 1D). The expression of CCL2 and its receptor (CCR2) was significantly up-regulated in the interaction between myeloid cells and fibroblasts within the knockout group. We examined the expression of various chemokines, including CCL2, based on the transcriptomic data (Fig S1), which revealed that, with the exception of CXCR4 and certain undetected chemokines and receptors, the expression levels of nearly all chemokines and their corresponding receptors in the HOM group were elevated compared to those in the WT group, including CCL2 and CCR2. These results suggest that in the absence of DCN, the expression of the CCL2-CCR2 axis in macrophages is strongly enhanced.

Negatively correlattion between DCN and CCL2 was found in colorectal cancer TAMs of human patients

We investigated the regulatory relationship between DCN and CCL2 in tumor-associated macrophages using an online database. Initial analysis via the TIMER database revealed thatthe presence of an excessive number of alternatively activated macrophages (M2) along with elevated CCL2 levels, was found to significantly shorten patient survival time (Fig 2A). Furthermore, data from the TISIDB database indicated a positive correlation between CCL2 expression in colorectal cancer and various immunosuppressive factors and immune checkpoints, including CD274 and TGF-β1 (Fig 2B). Additionally, analysis from the GEPIA database demonstrated a positive correlation between CCL2 and two immune checkpoints,

PD-1 and TIM-3 (Fig 2C).

We utilized the TIMER database to examine the relationship between DCN, CCL2, and the extent of immune infiltration by M2 macrophages, indicating that in the colorectal cancer tumor microenvironment, the expression of DCN is negatively correlated with the quantity of M2 macrophages (Fig 2D), whereas CCR2/CCL2 demonstrates a positive correlation with M2 macrophages. We employed TISCH, a database dedicated to single-cell sequencing, to validate the findings from our prior single-cell transcriptome sequencing analysis. In the three colorectal cancer single-cell sequencing datasets obtained from the database, we observed a significant correlation between DCN and CCL2 (Table 1), and found that CCL2 exhibited notably high expression levels specifically in macrophages within unilateral colorectal cancer samples, while the expression of DCN was found to be considerably low (Fig 2E). The above results indicate that during the occurrence of colorectal cancer, CCL2 can promote the M2 polarization of macrophages and is specifically highly expressed in TAMs, while the DCN expression level is low and negatively correlated with the number of M2 macrophages. In the case of co-expression of the two in the single-cell sequencing database, the correlation coefficient is high, suggesting that there may be a potential regulatory relationship between the two factors.

Gene	Gene2	Dataset	Celltype	Correlation
CCL2	*DCN*	CRC_GSE166555	All lineage	0.73
CCL2	*DCN*	CRC_EMTAB8107	All lineage	0.57
CCL2	*DCN*	CRC_GSE146771_Smartseq2	All lineage	0.45

Table1. Correlation Analysis of DCN and CCL2 in the TISCH Database

DCN inhibits the expression of factors associated with JAK2-STAT3 signaling pathway in TAMs .

In order to explore the specific mechanism of DCN regulating CCL2, we first used scRNA-seq to evaluate the transcription levels of all secreted cytokines, including CCL2, in myeloid cells in the HOM and WT groups, and found that there were significant differences in the expression of extracellular cytokines in the two groups. It is worth noting that the highly expressed cytokines in the HOM group, such as Hal, Hsp90aa1 and CCL24, are all related to the JAK-STAT signaling pathway[31-33] (Fig 3A). We then compared the main signaling pathways regulating the chemokine family between groups and found that except for the JAK-STAT signaling pathway, the trends between the other signaling pathways were not obvious (Fig 3B, Fig S2A-C). Therefore, we hypothesized that DCN might influence this pathway extracellularly, thus regulating CCL2 secretion in macrophages. To further elucidate the potential regulatory pathways connecting DCN and CCL2, we used the STRING database for analysis (Fig 3C), and the results were consistent with our initial hypothesis. Finally, we analyzed the co-expression relationship between CCL2 and JAK2-STAT3 signaling pathway in colorectal cancer through the TISIDB database (Fig 3D) and found that during the occurrence of colorectal cancer, the secretion of CCL2 from macrophages is positively correlated with the expression of JAK2 and STAT3. Collectively, this finding means that DCN may regulate CCL2 expression by inhibiting the JAK-STAT signaling pathway.

DCN can reduce M2 polarization of TAMs via suppressing secretion CCL2 in co-culture system

We performed targeted experiments to validate the findings obtained from single-cell sequencing and bioinformatics analyses. Initially, we established a co-culture system

comprising human peripheral blood mononuclear cells (THP-1) and colorectal cancer cells, as illustrated in Fig 4A. Following the induction of THP-1 cells into M0 macrophages using PMA, the cells were co-cultured with SW480 cells for a duration of 48 hours to generate tumor-associated macrophages. Microscopic examination revealed a morphological transformation of the tumor-associated macrophages to a spindle shape, in contrast to the M0 macrophages. qPCR analysis indicated an upregulation of CD206, IL-10, and TGF-β expression in the tumor-infiltrating macrophages, leading to a preliminary conclusion that the tumor-infiltrating macrophage model had been successfully established (Fig 4B, C). Under these experimental conditions, recombinant protein decorin was introduced exogenously. The qPCR results demonstrated a reduction in the transcription levels of the aforementioned genes following the addition of DCN, suggesting that DCN may influence the polarization of M0 macrophages into TAMs (Fig S3A). Furthermore, following the exogenous administration of DCN, We verified the downregulation of CCL2 protein and transcription levels by qPCR and WB experiments in the co-culture system of SW480 and SW620 (Fig 4D, E， Fig S3B).

We collected the culture medium from the transwell system and conducted ELISA assays (Fig 4F,Fig S3C-D). The findings indicated that in the co-culture system involving the colorectal cancer cell lines SW480, SW620, and HCT116, there was a marked increase in CCL2 secretion by TAM. On contrast, this increase was notably inhibited following the exogenous introduction of DCN. We used a transwell system to determine if DCN affect CCL2-mediated tumor cell migration, and positioned M0 macrophages in the upper chamber of the transwell apparatus, while placing TAMs culture medium in the lower chamber. We added CCL2 antibody to the transwell culture medium as a positive control. The results of

crystal violet staining demonstrated that TAM-conditioned medium significantly enhanced the recruitment of M0 macrophages. Furthermore, the presence of DCN was found to inhibit this recruitment, thereby suggesting that DCN exerts its effects by downregulating CCL2 expression in TAM (Fig 4G). ELISA detection of the culture medium also observed a decrease in CCL2 expression (Fig 4H). The above results indicate that DCN can inhibit the migration of macrophages induced by the CCL2 pathway in TAMs. We utilized fluorescent antibodies to label CCR2 and observed a significant reduction in fluorescence intensity upon the exogenous addition of DCN (Fig 4I). Through the above experiments, we verified in vitro that DCN can inhibit the secretion of CCL2 in TAMs in the colorectal cancer tumor microenvironment, which is consistent with the previous results of single-cell sequencing and online database mining.

In order to explore the effect of reduced CCL2 expression in TAMs on colorectal cancer cells, we constructed a DCN-overexpressing macrophage cell line and confirmed the high expression of DCN in TAMs by qPCR experiments (Fig S4). After co-culture with colorectal cancer cells by transwell system for 48 hours, the changes in the expression levels of immune checkpoints in colorectal cancer cells were observed. WB results showed that the expression of immune checkpoint PD-L1 was reduced, and the phosphorylation level of AKT-MAPK (p38), which mainly regulates PD-L1 expression (Fig 4J), was reduced, all three types of colorectal cancer cells exhibited varying degrees of apoptosis in a co-culture system overexpressing DCN-TAMs (Fig S5). indicating that colorectal cancer cells may be more difficult to activate the immune checkpoint autophagy process of macrophages, and thus more difficult to escape immune function. The above results indicate that increased expression levels of DCN will

affect the process of TAMs recruiting M0 macrophages to migrate, and affect polarization to M2 macrophages, thereby enhancing the immune surveillance of colorectal cancer cells by macrophages.

TLR2 was indetified as a crucial junction for DCN inhibiting CCL2 secretion in TAMs

To elucidate the specific mechanisms by which DCN regulates CCL2, the M0 macrophages overexpressing DCN were co-cultured with SW480 for a duration of 48 hours. Western blot analysis revealed that, in comparison to the control group, the expression levels of CCL2 and CCR2 were significantly diminished, alongside a reduction in the phosphorylation levels of JAK2 and STAT3. These findings suggest that the JAK2-STAT3 signaling pathway is inhibited following DCN overexpression, which in turn influences the expression of CCL2 and CCR2 (Fig 5A,Fig S6).

To identify the direct target of DCN in regulating the JAK-STAT signaling pathway extracellularly, we conducted immunoprecipitation-mass spectrometry (IP-MS) analysis to ascertain the membrane protein receptors potentially influenced by DCN. Mass spectrometry analysis detected a total of 2805 proteins, and GO analysis showed that 1081 of them were membrane proteins. In conjunction with prior findings that DCN inhibits the expression of the JAK2-STAT3 signaling pathway in tumor-infiltrating macrophages, the identified proteins were enriched. Table 2 presents the proteins that may interact with DCN. Among them, TLR2 was considered in previous studies to be an important receptor regulating the secretion of the macrophage chemokine family[34-36]. Hence, we proceeded protein docking and followed with co-immunoprecipitation (co-IP) experiments involving DCN and TLR2, co-IP results

corroborated the interaction between DCN and TLR2 (Fig 5C). Through protein-protein interaction analysis conducted in PyMOL, we screened all potential functional residues and categorized them based on their interactions. Notably, multiple groups of residues were found to form hydrogen bonds between TLR2 and DCN, including a hydrogen bond between LYS37 of TLR2 and ASN255 of DCN. The interaction score for the TLR2-DCN complex was -751, indicating a favorable interaction (Fig 5D). We also performed molecular dynamics simulations on the protein docking model and observed that under the condition of a step length of 100ns, during the simulation, the RMSD of the protein finally stabilized between 3.5-4.0 Å. This shows that the protein has a small degree of fluctuation relative to the initial conformation, indicating that the conformations of the two are relatively stable (Fig S7). Spatial localization studies conducted via confocal microscopy revealed a high degree of overlap in the spatial distribution of these two proteins, thereby further substantiating the aforementioned conclusions (Fig 5E).

To delve into the potential dependence of DCN on TLR2 in the modulation of CCL2 secretion, we utilized siRNA to downregulate TLR2 expression in TAMs that overexpress DCN . Western blot analysis revealed an upregulation of CCL2 expression in comparison to the control group, alongside an increase in p-STAT3 levels. The above results indicate that DCN may bind to the functional residues of TLR2, inhibit the activation of the JAK2-STAT3 signaling pathway downstream of TLR2, and thus down-regulating the expression of CCL2 in TAMs (Fig 5F,Fig S8).

Protein Group	Protein ID	Gene Names	Accession	-10lgP
219	428	EGFR ERBB ERBB1 HER1	P00533	243.74
1339	1608	METAP2 MNPEP P67EIF2	P50579	107.56
1890	1594	METAP1 KIAA0094	P53582	92.24
2686	2729	SLTM MET	Q9NWH9	89.13

21	12	P4HB ERBA2L PDI PDIA1 PO4DB	P07237	323.51
386	314	SERBP1 PAIRBP1 CGI-55	Q8NC51	211.47
486	323	IGF2R MPRI	P11717	199.22
937	727	IGF2BP2 IMP2 VICKZ2	Q9Y6M1	156.31
1731	1556	FCGR1A FCG1 FCGR1 IGFR1	P12314	86.48
4137	3692	FCGR2C CD32 FCG2 IGFR2	P31995	27.96
2603	2188	TLR2 TIL4	O60603	47.35

Table2. Enrichment Results for Membrane Proteins and the JAK-STAT Signaling Pathway from IP-MS Experiments

DCN supresses tumor growth by inhibiting the secretion of CCL2 of TAMs in exograft mice

In order to verify whether the overexpression of DCN in TAMs can affect the expression of CCL2 in TAMs and inhibit the occurrence and development of CRC, we designed a DCN overexpression vector targeting TAMs with reference to previous studies, inserted the promoter of Mrc1 (CD206) before the DCN sequence to target TAMs[37], and inserted a flag tag into the DCN sequence to mark it, inducing TAMs to overexpress DCN. We used CT26 cells to construct a mouse subcutaneous solid tumor model. When the solid tumor volume was about 100mm^3, the mice were injected with DCN overexpression lentivirus by tail vein injection. The mice were supplemented every 72h, and were killed after 10 days of culture. The solid tumors were removed for subsequent experiments (Fig 6A). After the mice were killed, it was found that the solid tumors in the DCN lentivirus treatment group were lower than those in the control group (Fig 6B), which was also confirmed by the growth curve of the solid tumors in mice cultured for 10 days. HE staining of solid tumors revealed that the solid tumor tissue in the treatment group was loose and the necrosis was more severe than that in the control group (Fig 6C). Immunohistochemical analysis of tumor sections revealed that the expression of CD206, IL-10, and TGF-β, markers of M2 polarization, was downregulated in

tissues (Fig S9, Fig 6D), and CCL2 expression was downregulated. We analyzed the purity of the extracted TAMs by flow cytometry. We found that $CD206^{+}CD11b^{+}$ cells in the control group accounted for more than 80% of the total, indicating that the sample purity was high, but $CD206^{+}$TAMs in the DCN treatment group were downregulated, which once again proved that DCN treatment inhibited the M2 polarization of TAMs (Fig 6E,Fig S10). We then performed qPCR and WB analysis on the extracted TAMs, and confirmed the presence of DCN overexpression in TAMs at the transcriptional and protein levels, proving that the lentivirus we designed can target TAMs in solid tumors and induce TAMs to overexpress DCN. We also observed downregulation of the JAK2-STAT3 signaling pathway and CCL2 expression, which is consistent with our previous in vitro experimental results (Fig 6F, Fig 6G,Fig S11). Finally, we observed the distribution of DCN and TLR2 in the tumor by immunofluorescence experiments, and found that compared with the control group, the DCN treatment group showed stronger expression of DCN and TLR2, and their spatial distribution was highly overlapped (Fig 6H), further confirming that DCN can inhibit the expression of CCL2 through TLR2 inhibiting the JAK2-STAT3 signaling pathway, thereby inhibiting the M2 polarization of TAMs in vivo.

DCN synergistic with PD-1 immune checkpoint inhibitors to inhibit colorectal cancer

To explore whether DCN-overexpressing TAMs can be combined with PD-1 immune checkpoint inhibitors to inhibit tumor progression through immunotherapy, we combined the DCN-overexpressing lentivirus targeting TAMs with PD-1 inhibitors (PD-1-IN-17) to treat mice with colorectal cancer models to explore whether it can inhibit immune escape and activate

the antigen presentation pathway.

After three consecutive administrations of the drug at 72-hour intervals, tumor tissue and peripheral blood were collected from the mice for subsequent experiments. We first found that both DCN and PD-1 inhibitor treatment effectively inhibited tumor growth in mice, with the combination treatment group showing the most pronounced inhibitory effect (Fig 7A). HE staining revealed necrosis in tumors in the DCN, immune checkpoint inhibitor, and combination groups, while tumors in the control group were relatively dense (Fig7 B). We first confirmed the downregulation of PD-1 expression in tumors using immunohistochemical staining and flow cytometry (Fig S12A,Fig S12B). Subsequent immunohistochemical results showed that the pro-tumor factor KI67 was significantly downregulated in the DCN group, PD-1 inhibitor group, and combination therapy group, while the tumor suppressor factor P27 was significantly upregulated in all three groups (Fig 7C). We also found that the tumor suppressor factor MLH1, which responds to PD-1 inhibitors, was upregulated in the PD-1 inhibitor group and the combination therapy group (Fig S12C). Flow cytometry analysis showed that, compared with the control group, tumor cells in the DCN group, PD-1 inhibitor group, and combination therapy group all exhibited a certain degree of apoptosis, with the most severe apoptosis in the combination therapy group. These results indicate that the combined application of DCN-overexpressed TAM and PD-1 inhibitors can inhibit tumor growth and kill tumor cells (Fig S13).

Regarding antigen presentation, flow cytometric analysis of tumor cells revealed significantly increased MHC class I expression in both the DCN and PD-1 inhibitor-treated groups compared to the control group, with the combination group showing the highest MHC

class I expression (Fig 7D). Furthermore, the proportion of MHC class I- and MHC class II-positive macrophages in the combination group was significantly increased compared to the DCN-treated and PD-1 inhibitor-treated groups, suggesting that the combined administration of DCN and PD-1 inhibitors can enhance macrophage antigen presentation and activate tumor-killing immune cells (Fig 7E). Flow cytometric analysis of peripheral blood from mice revealed a significant increase in the proportion of $CD8^+$ T cells and a decrease in the proportion of Treg cells in the combination group, suggesting that the combined administration of DCN and PD-1 inhibitors enhances antigen presentation from tumor cells to macrophages, thereby activating $CD8^+$ T cells to kill tumor cells (Fig 7F, Fig S14).

Discussion

Currently, the depolarization of M2 TAMs has emerged as one of the key strategies in tumor immunotherapy; notably, CCL2 serves as a critical factor in M2 polarization within TAMs, actively promoting both macrophage recruitment and the development of their immunosuppressive phenotype.CCL2 serves not only as a pivotal chemokine for recruiting monocytes and macrophages but also acts as a key driver of their polarization toward the M2 phenotype[38], while simultaneously promoting angiogenesis, immunosuppression, and tumor metastasis—thereby playing a central role in the progression of solid tumors, such as colorectal cancer[39,40]. Currently, the suppression of CCL2-induced TAM reprogramming has emerged as a key strategy in cancer immunotherapy. Studies across esophageal squamous cell carcinoma[41], hepatocellular carcinoma[18], and non-small cell lung cancer[19] have demonstrated that inhibiting CCL2 secretion leads to TAM depolarization, thereby

suppressing tumor progression. Most of these studies focus on regulating CCL2 secretion through intracellular lncRNAs or Intracellular Signaling Factors[42]; our study, however, establishes for the first time a direct link between the extracellular regulation of the CCL2 axis by DCN within tumor-associated macrophages (TAMs) in colorectal cancer.

CCL2 is primarily regulated by the AKT-PI3K and JAK-STAT signaling pathways[43,44]. Previous single-cell sequencing results revealed alterations in the transcriptional levels of the JAK-STAT signaling pathway family following DCN knockout; we therefore hypothesize that the macrophage JAK-STAT signaling pathway may regulate CCL2 secretion. Suppression of CCL2 secretion in the tumor microenvironment via nanomaterials[45] or strategies[46] targeting the CCL2 signaling pathway can effectively ameliorate the immunosuppressive tumor microenvironment and enhance the cytotoxic activity of immune cells. Our study provides a new therapeutic strategy for inhibiting cancer progression by suppressing CCL2 secretion in TAMs.

Immune checkpoint inhibitors targeting the PD-1/PD-L1 axis have revolutionized cancer immunotherapy, yet their efficacy in CRC remains largely confined to the ~15% of patients with microsatellite instability-high or mismatch repair-deficient tumors, which are characterized by high tumor mutational burden and robust immune infiltration[47]. In stark contrast, the vast majority of CRC cases are microsatellite-stable or mismatch repair-proficient and exhibit an immunosuppressive TME with sparse T-cell infiltration and abundant TAMs, rendering them largely refractory to single-agent PD-1 blockade[48]. The objective response rate in MSS CRC remains below 5%[49], underscoring an urgent unmet need to overcome ICI resistance in this population. Combination therapies involving CCL2-

590 blocking ICIs have yielded positive results in esophageal[50], bladder[51], and breast cancers[52].
591 Due to the immunosuppressive status of immune-excluded and immune-desert colorectal
592 cancer, ICIs confer modest benefit. Our research offers a new strategy to reverse the
593 immune-excluded microenvironment and improve the response to colorectal cancer
594 immunotherapy.

595 Several limitations of this study should be acknowledged. Although IP-mass spectrometry
596 suggested that DCN may interact with TLR2 to inhibit downstream JAK2/STAT3 signaling,
597 whether DCN regulates STAT3 signaling through other membrane proteins remains
598 unexplored, and the DCN-TLR2 interaction currently relies on protein docking and molecular
599 dynamics simulations without experimental evidence such as protein crystallization.
600 Cross-linking MS or protein crystallization may provide structural evidence for the DCN-TLR2
601 binding interface. Second, although TAMs overexpressing DCN enhanced the efficacy of
602 immune checkpoint inhibitors in colorectal cancer, the use of engineered TAMs as a cell
603 therapy faces substantial challenges for clinical translation. Alternative strategies such as
604 nanocarriers (e.g., liposomes, exosomes) or antibody-drug conjugates that deliver DCN
605 specifically to tumor-associated macrophages (e.g., via CD163- or MRC1-targeted
606 DCN-nanocomplexes) could achieve in situ reprogramming without ex vivo manipulation,
607 thereby improving the translational potential of this therapeutic approach.

608 In this investigation, we employed single-cell transcriptome sequencing to analyze the
609 activation of the JAK-STAT signaling pathway in macrophages derived from DCN-deficient
610 and wild-type mice. Our findings indicate that the absence of DCN correlates with elevated
611 levels of CCL2 expression. Furthermore, we validated this observation using an online

612 database, suggesting that a comparable phenomenon occurs in tumor-associated
613 macrophages within human colorectal cancer. Concurrently, we utilized methodologies from
614 cell biology and molecular biology to elucidate the specific mechanisms by which DCN
615 modulates CCL2 expression. Our results indicate that DCN may influence the intracellular
616 JAK2-STAT3 signaling pathway via the TLR2 receptor present on the macrophage membrane,
617 thereby inhibiting CCL2 expression and subsequently reducing the recruitment of peripheral
618 blood and tissue-resident macrophages. Furthermore, we verified through in vivo experiments
619 that DCN-overexpressing TAMs can inhibit CCL2 expression in vivo, thereby inhibiting the
620 polarization of M2 TAMs, and can be combined with PD-1 inhibitors to inhibit tumorigenesis.
621 This study demonstrates that DCN can impede the recruitment and polarization effects of
622 TAMs on macrophages, thereby enhancing the cytotoxic functions of immune cells within the
623 tumor microenvironment, representing a novel target for immunotherapeutic strategies for
624 colorectal cancer.
625

Conflicts of interest

The authors declare they have no known competing financial interests or personal relationships that could have appeared to influence the work reported in this paper.

Acknowledgments

This work was supported by the Fund of the National Key Research and Development Project of MOST, the National Natural Science Foundation of China (82470005), the Affiliated Xiangshan Hospital of Wenzhou Medical University, and Wenzhou Institute University of Chinese Academy of Sciences. We thank members in the Wu lab for providing the help, and critical comments

Author Contributions

X.-D.C, Z.-Q.F. and Q.L. performed the data analysis. X.-D.C,Y L and L.-L.C. wrote the initial draft of this manuscript. Y.Z., J.W., and C.Z. offered numerous suggestions during the writing of the article. X.-L.B. and M.W. conceived the project and supervised overall experiments. All the authors participated in editing both the form and content of this manuscript and approved the final version.

Data availability

Not applicable.

Ethics approval

Not applicable.

651

652

653

654

655

656

657

658

Figure Legends:

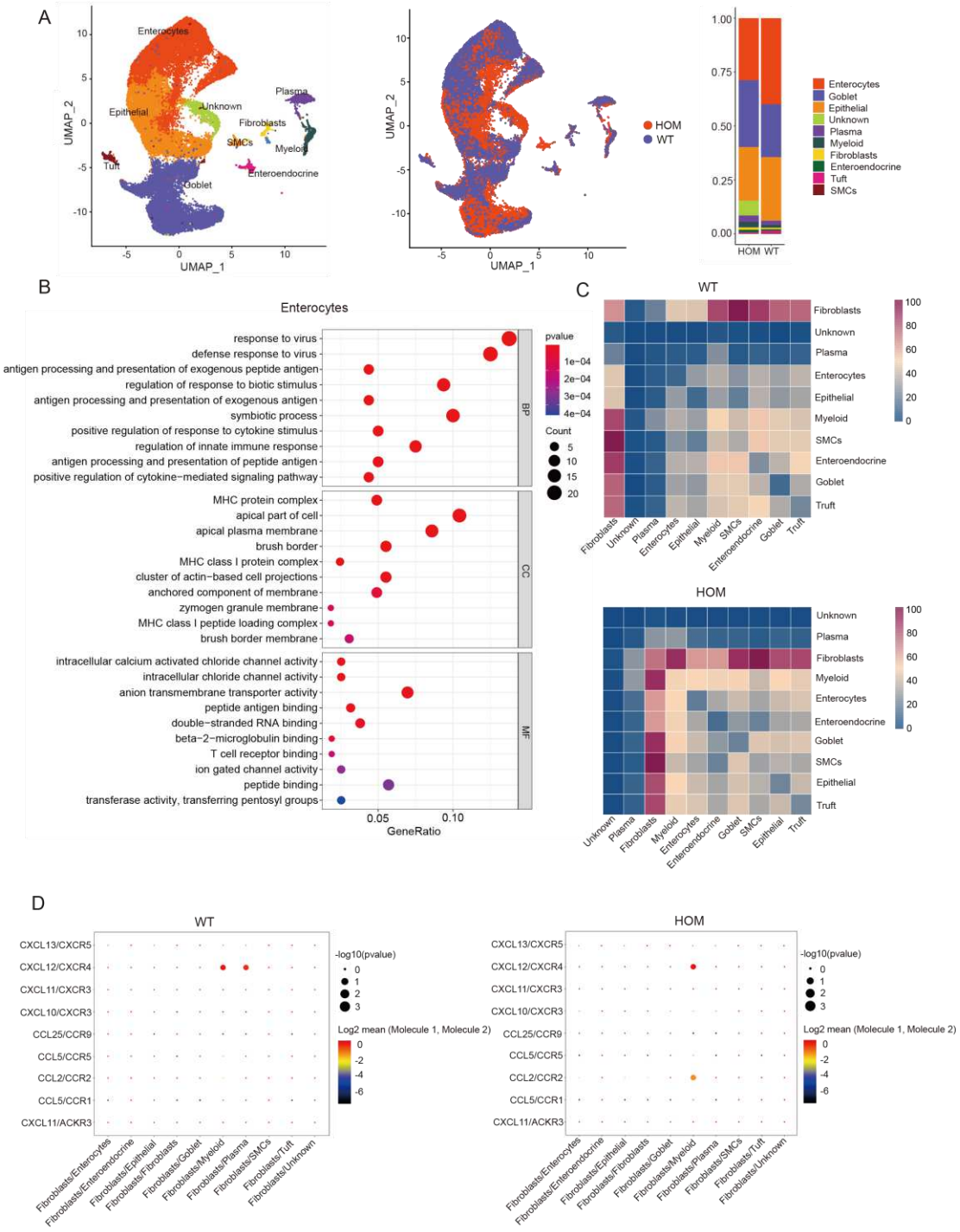


Fig 1. Single-cell sequencing analysis reveals a role of DCN in colonic immune cells from DCN knockout and wild-type mice. (A) clustering results by sample. (B) GO analysis results of functional enrichment of enterocytes. (C) Cell-to-cell interaction in WT and DCN knockout group. (D) Cell-cell interaction pairs with higher expression in HOM group. 3 mice per group .

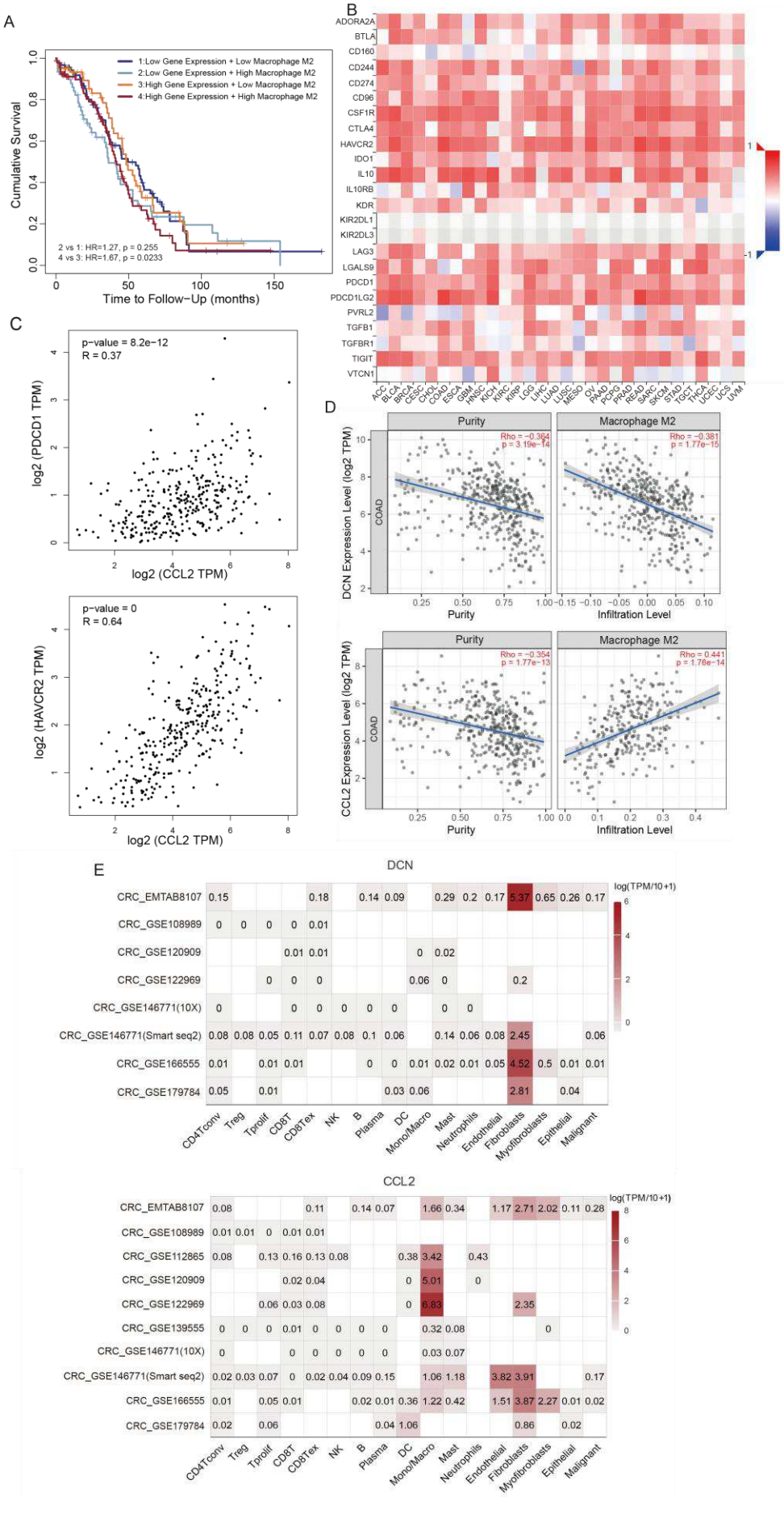

A
1:Low Gene Expression + Low Macrophage M2
2:Low Gene Expression + High Macrophage M2
3:High Gene Expression + Low Macrophage M2
4:High Gene Expression + High Macrophage M2
Cumulative Survival
2 vs 1: HR=1.27, p = 0.255
4 vs 3: HR=1.67, p = 0.0233
Time to Follow−Up (months)
B
ADORA2A
BTLA
CD160
CD244
CD274
CD96
CSF1R
CTLA4
HAVCR2
IDO1
IL10
IL10RB
KDR
KIR2DL1
KIR2DL3
LAG3
LGALS9
PDCD1
PDCD1LG2
PVRL2
TGFB1
TGFBR1
TIGIT
VTCN1
C
p−value = 8.2e−12
R = 0.37
log2 (PDCD1 TPM)
log2 (CCL2 TPM)
p−value = 0
R = 0.64
log2 (HAVCR2 TPM)
log2 (CCL2 TPM)
D
Purity
Macrophage M2
Rho = −0.364
p = 3.19e−14
Rho = −0.381
p = 1.77e−15
COAD
DCN Expression Level (log2 TPM)
Purity
Infiltration Level
Rho = −0.354
p = 1.77e−13
Rho = 0.441
p = 1.76e−14
CCL2 Expression Level (log2 TPM)
E
DCN
log(TPM/10+1)
CRC_EMTAB8107
CRC_GSE108989
CRC_GSE120909
CRC_GSE122969
CRC_GSE146771(10X)
CRC_GSE146771(Smart seq2)
CRC_GSE166555
CRC_GSE179784
CD4Tconv
Treg
Tprolif
CD8T
CD8Tex
NK
B
Plasma
DC
Mono/Macro
Mast
Neutrophils
Endothelial
Fibroblasts
Myofibroblasts
Epithelial
Malignant
CCL2
log(TPM/10+1)
CRC_EMTAB8107
CRC_GSE108989
CRC_GSE112865
CRC_GSE120909
CRC_GSE122969
CRC_GSE139555
CRC_GSE146771(10X)
CRC_GSE146771(Smart seq2)
CRC_GSE166555
CRC_GSE179784

Fig 2. Online database analysis unveils the role of CCL2 in the development of colorectal cancer. (A) High expression of CCL2 is related to the low survival rate of patients. (B) CCL2 is positively correlated with various immunosuppressive factors in colorectal cancer. (C) CCL2 and PD- 1 and TIM-3 are positively correlated with two immune checkpoints. (D) Correlation between CCL2 or DCN and immune infiltration of M2 macrophages in colorectal cancer. (E) The expression of CCL2 in various types of colorectal cancer cells .

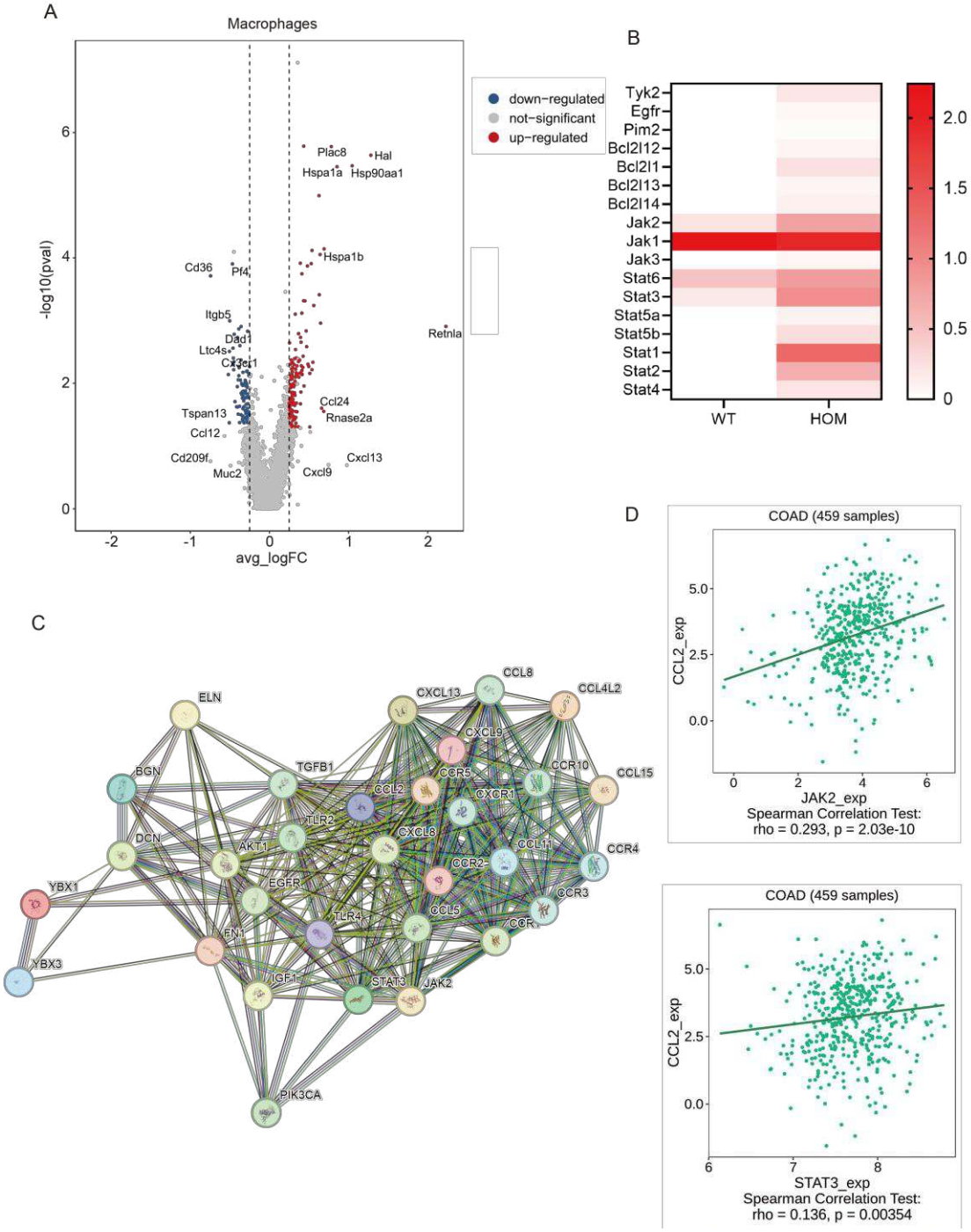


Fig 3Single-cell transcriptome analysis of the specific mechanism of DCN regulating CCL2. (A) Differences in secretion factors of myeloid cells between HOM and WT groups. (B) Heat map of differences in intracellular signaling pathways in

macrophages between HOM and WT groups. (C) String predicts the regulatory network of DCN and CCL2. (D) Analysis of the correlation between CCL2, JAK2 and STAT3 expressions in colorectal cancer macrophages using TISCH database.

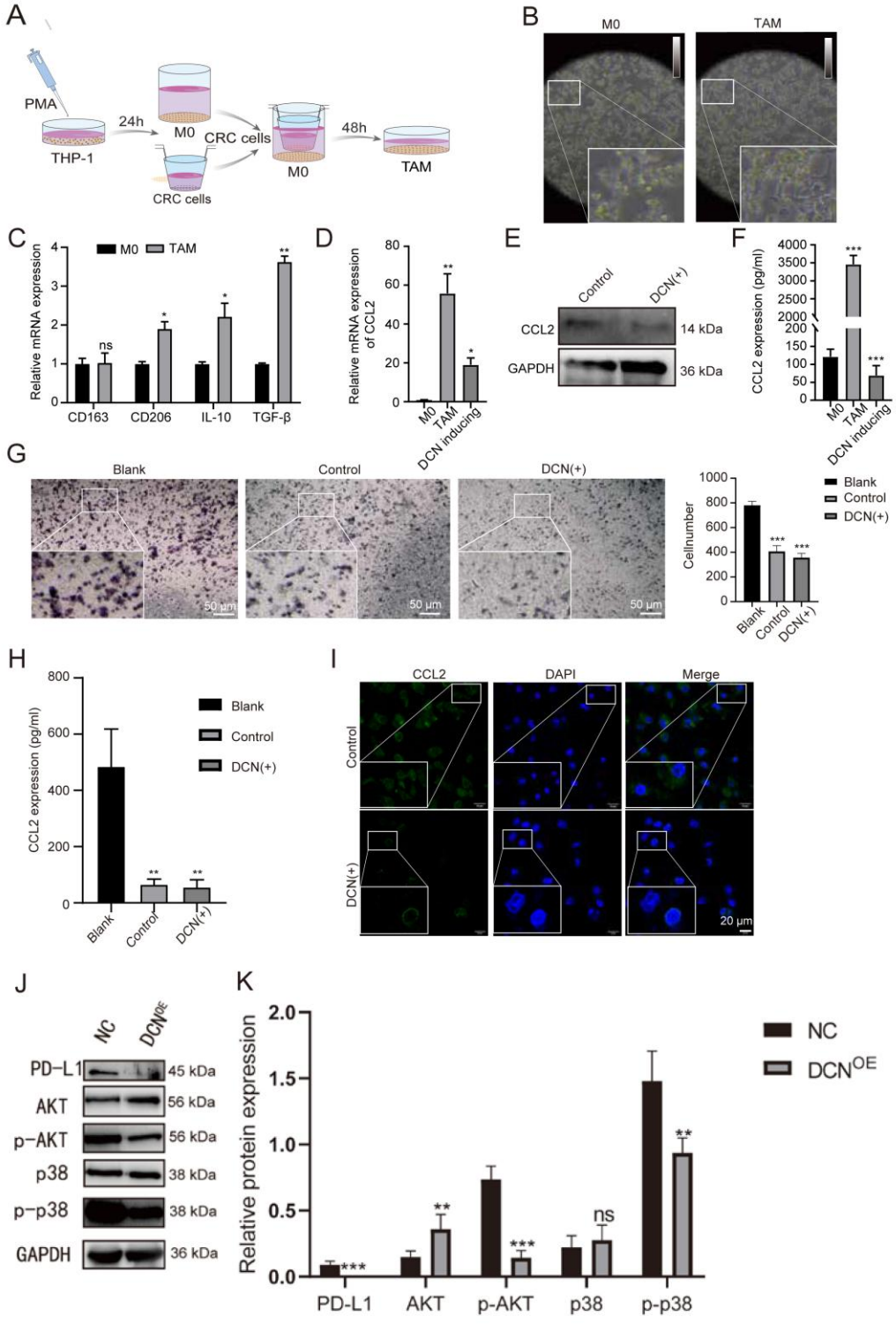


Fig 4. Exogenous addition of DCN reduces the expression of CCL2 in TAMs (A) Schematic diagram of the tumor-associated macrophage modeling process. (B) Observation of TAM morphological changes under a microscope. (C) qPCR detection of TAM markers to verify this modeling process. Data are presented as mean ± SD, n

= 3 per group. One-way ANOVA was used. *p < 0.05, **p < 0.01, ***p< 0.001 vs M0 ns indicates no significant difference. (D) Detection of changes in CCL2 transcription levels in TAMs by qPCR. Data are presented as mean ± SD, n = 3 per group. One-way ANOVA was used. *p < 0.05, **p < 0.01vs M0. (E) Western blot analysis of CCL2 protein level changes in TAM. (F) ELISA assay to detect extracellular secretion of CCL2 in TAMs. Data are presented as mean ± SD, n = 3 per group. One-way ANOVA was used. *p < 0.05, **p < 0.01, ***p< 0.001 vs M0. (G) Transwell assay to observe the migration of M0 macrophages. Scale bar : 50μm. Data are presented as mean ± SD, n = 3 per group. One-way ANOVA was used. *p < 0.05, **p < 0.01, ***p< 0.001 vs Blank. (H) ELISA detection of CCL2 content in transwell culture medium. Data are presented as mean ± SD, n = 3 per group. One-way ANOVA was used. *p < 0.05, **p < 0.01 vs Blank (I) Immunofluorescence experiment was used to observe the expression of CCR2 receptor in TAMs. Scale bar : 20μm. (J) WB detection of changes in PD-L1 and AKT-MAPK (p38) signaling pathway protein levels in SW480 cells.

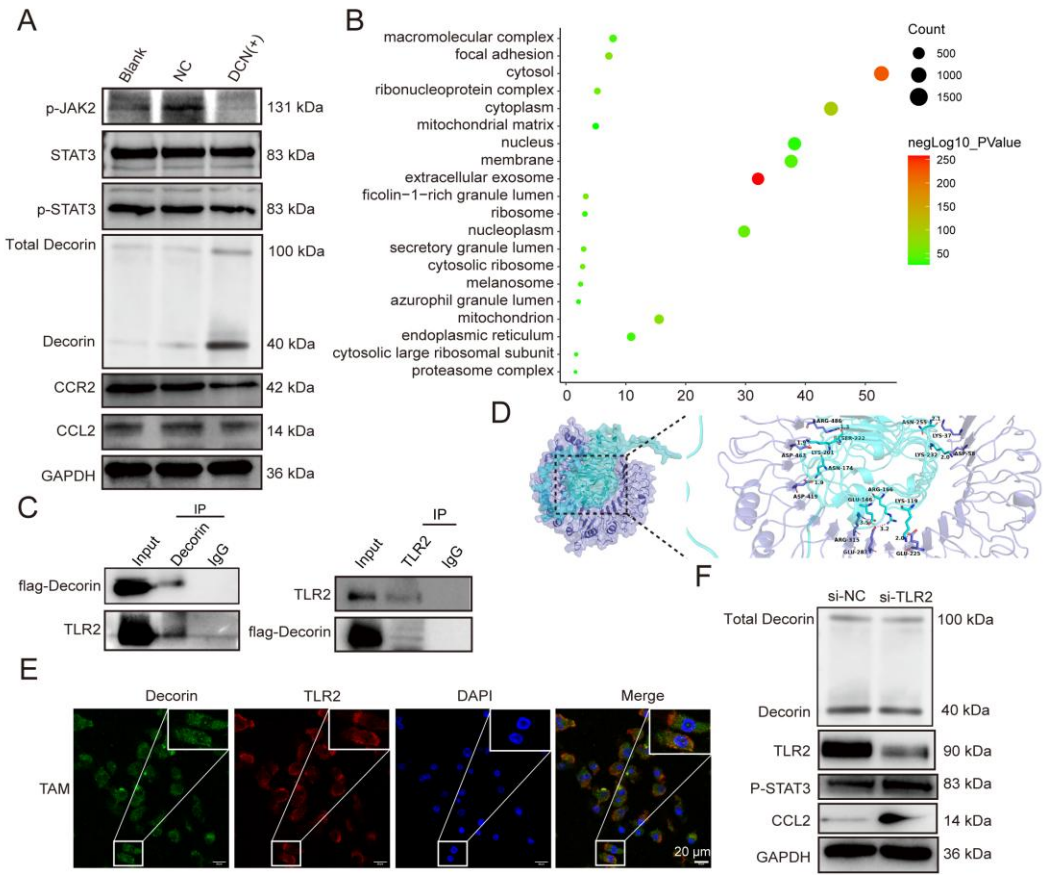


Fig 5. DCN inhibits the secretion of CCL2 in TAMs by binding to TLR2 and inhibiting downstream JAK-STAT activation. (A) qPCR detection of DCN overexpression in TAMs. (B) Western Blot detection of JAK-STAT signaling pathway activation in DCN-overexpressing TAMs. （C）IP-MS analysis of DCN interaction targets on cell membrane surface.（D）Auotodock mimics the binding site of TLR2 and DCN.（E）Co-IP assay to detect the interaction between DCN and TLR2.（F）Immunofluorescence experiments to detect the spatial distribution of DCN and TLR2

in TAMs. (G) After siRNA interfered with TLR2 expression, WB was used to detect the changes in CCL2 expression under DCN overexpression conditions. Scale bar represents 20 μm.

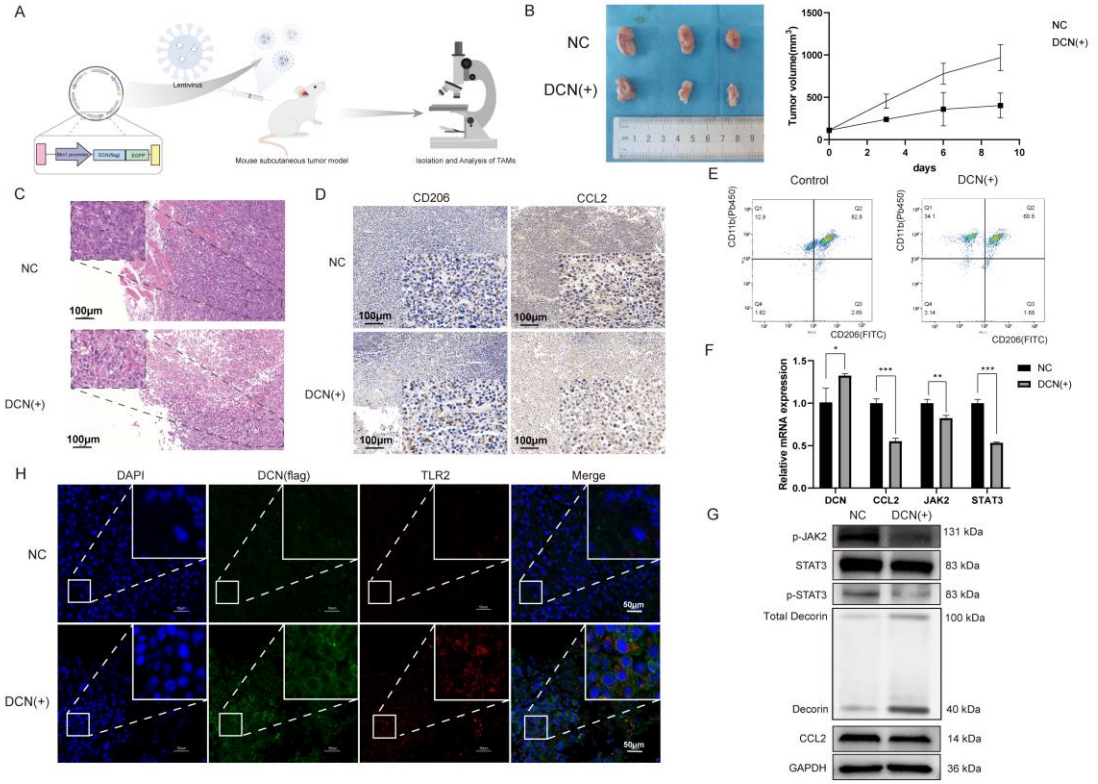


Fig 6. DCN-overexpressing TAMs can suppress the immunosuppressive activity of TAMs within murine CRC in a subcutaneous tumor model. (A) DCN-targeted TAMs treatment of subcutaneous tumor model in mice. (B) Changes in tumor size and volume of mice in the DCN treatment group and the control group. Data are presented as mean ± SD, n = 3 per group. One-way ANOVA was used. *p < 0.05, **p < 0.01 vs NC. (C) HE staining to observe the pathological changes of tumor in mice treated with DCN and in the control group. (D) Immunohistochemical staining was used to observe the changes in the expression levels of CD206 and CCL2 in tumor-bearing tissues between the DCN treatment group and the control group. (E) Flow cytometry was used to observe the changes of TAMs surface markers in the treatment group and the control group. (F) qPCR was used to detect the changes in transcription levels of DCN and related signaling pathways in the DCN treatment group. Data are presented as mean ± SD, n = 3 per group. One-way ANOVA was used. *p < 0.05, **p < 0.01, ***p< 0.001 vs NC. (G) WB was used to detect the changes in the levels of DCN and CCL2-related signaling pathway proteins in the DCN treatment group. (H) Immunofluorescence tissue staining was used to observe the expression of DCN in TAMs and the spatial distribution of DCN and TLR2 in the DCN treatment group and the control group.

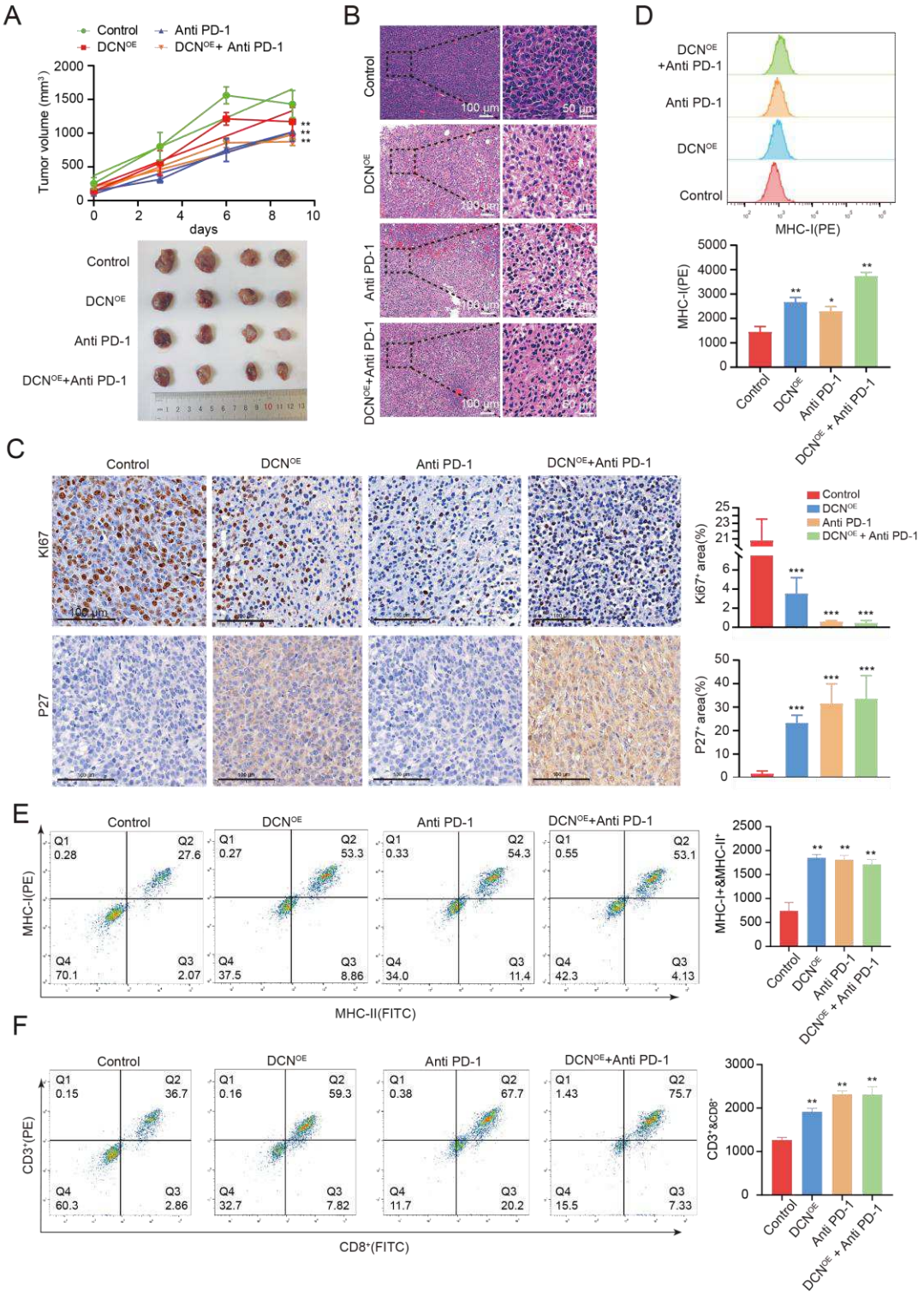


Fig 7. Combination therapy with DCN-overexpressing TAMs and PD-1 inhibitors inhibits immune evasion in murine CRC (A) Changes in tumor size and volume in mice treated with DCN overexpression combined with PD-1-IN-17, compared to the control group. Data are presented as mean ± SD, n = 3 per group. One-way ANOVA was used. *p < 0.05, **p < 0.01 vs Control. (B) HE staining to observe the pathological changes of tumor in mice treated withDCN overexpression combined with PD-1-IN-17 and in the control group. (C) Immunohistochemical staining was

used to observe the changes in the expression levels of Ki67 and P27 in tumor-bearing tissues between the DCN overexpression combined with PD-1-IN-17 and in the control group. Data are presented as mean ± SD, n = 3 per group. One-way ANOVA was used. *p < 0.05, **p < 0.01, ***p< 0.001 vs Control. (D) Flow cytometry was used to observe changes in PD-1 expression within tumor tissues in the treatment and control groups. Data are presented as mean ± SD, n = 3 per group. One-way ANOVA was used. *p < 0.05, **p < 0.01 vs Control. (E) Flow cytometry analysis was employed to assess changes in the proportions of MHC I^+ and MHC II^+ macrophages within tumor tissues—specifically examining the group treated with a combination of PD-1 inhibitors and DCN overexpression, in comparison to the control group. Data are presented as mean ± SD, n = 3 per group. One-way ANOVA was used. *p < 0.05, **p < 0.01 vs Control. (F) Flow cytometry was employed to analyze changes in the proportion of $CD8^+$ T cells within tumor tissues—specifically comparing the group treated with a combination of PD-1 inhibitors and DCN overexpression against a control group. Data are presented as mean ± SD, n = 3 per group. One-way ANOVA was used. *p < 0.05, **p < 0.01 vs Control.

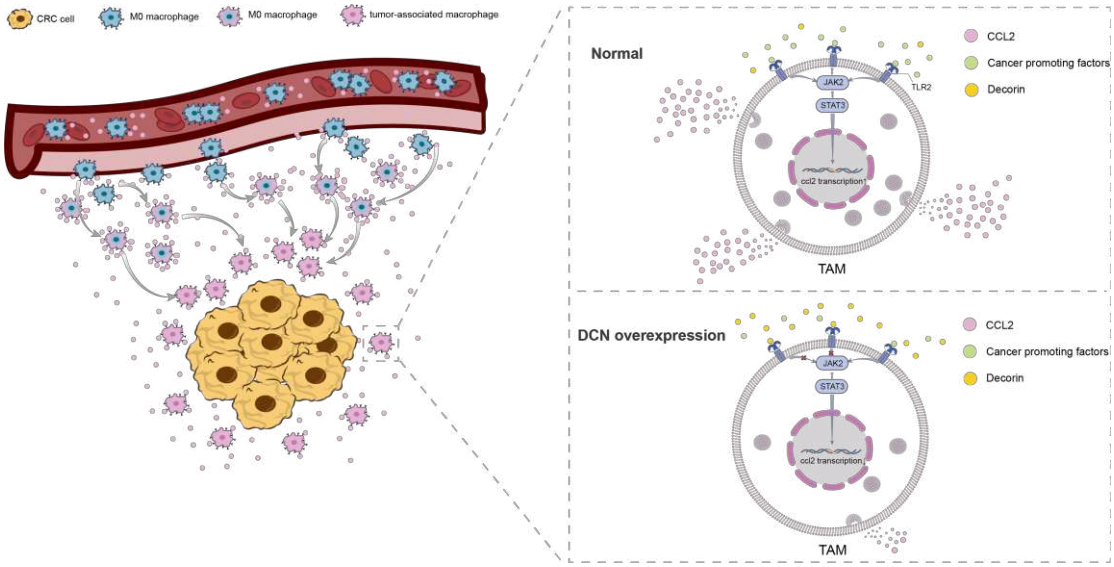
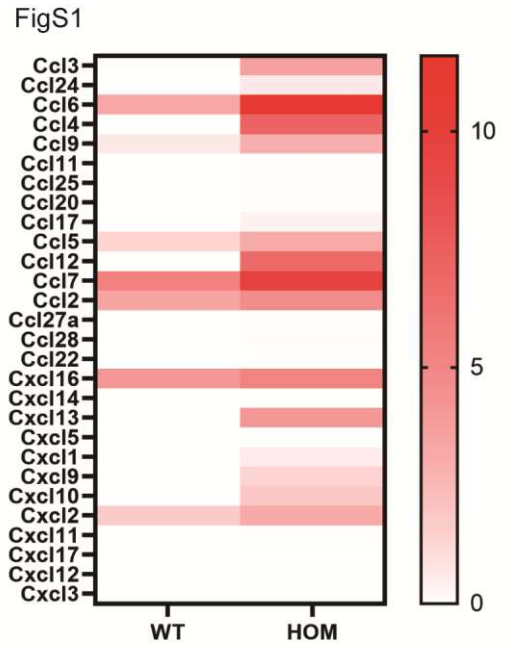


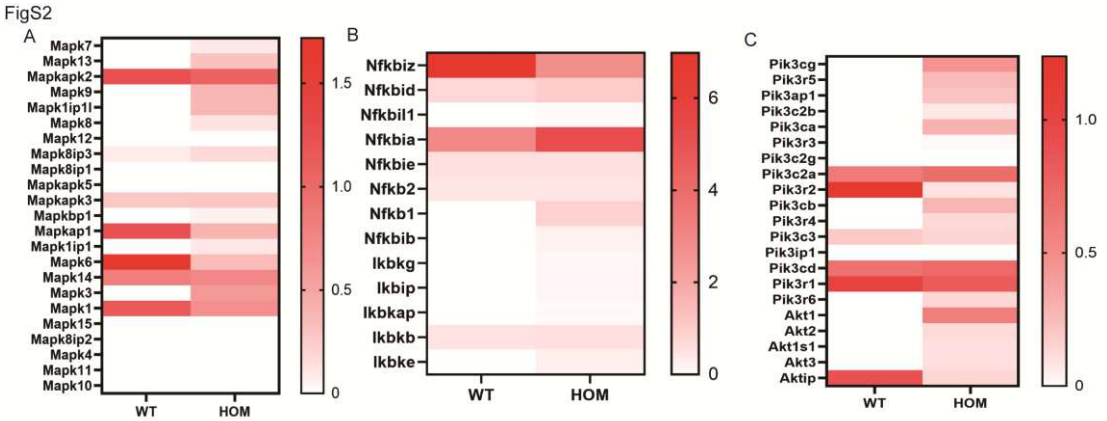
Fig 8. The specific mechanisms by which DCN regulates CCL2 secretion in M2-type TAMs in the extracellular environment

Supplymental Figure Legends:



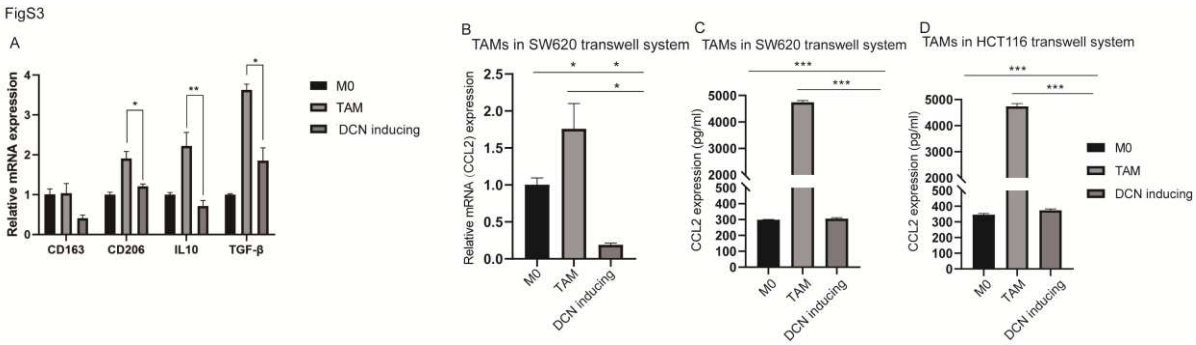
760

761 FigS1: Differential expression analysis of chemokine family genes at the
762 transcriptional level.



763

764 FigS2: Differences in transcription levels of chemokine family signaling pathways
765 between the HOM group and the WT group; A. Changes in transcription levels of the
766 MAPK signaling pathway; B. Changes in transcription levels of the NF-κB signaling
767 pathway; C. Changes in transcription levels of the JAK-STAT signaling pathway.

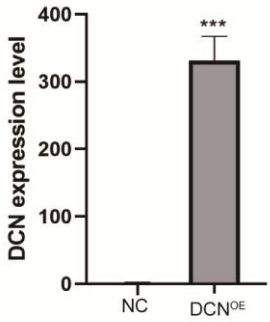


768

769 FigS3: A. Expression of M2-type TAM markers after exogenous DCN addition; B.
770 qPCR analysis of changes in CCL2 transcription levels in TAMs induced by SW620

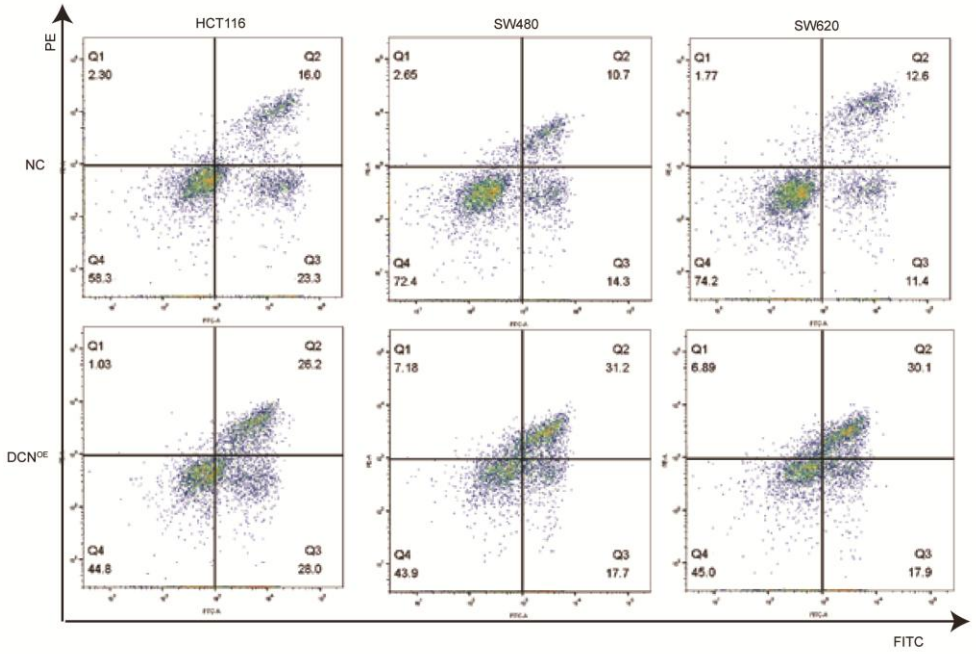
after exogenous DCN addition; C. The effect of exogenous DCN addition on CCL2 protein secretion levels in SW620 co-cultured TAMs; D. The effect of exogenous DCN addition on CCL2 protein secretion levels in HCT116 co-cultured TAMs; "*" indicates P < 0.05, "**" indicates P < 0.01, and "***" indicates P < 0.001;

FigS4



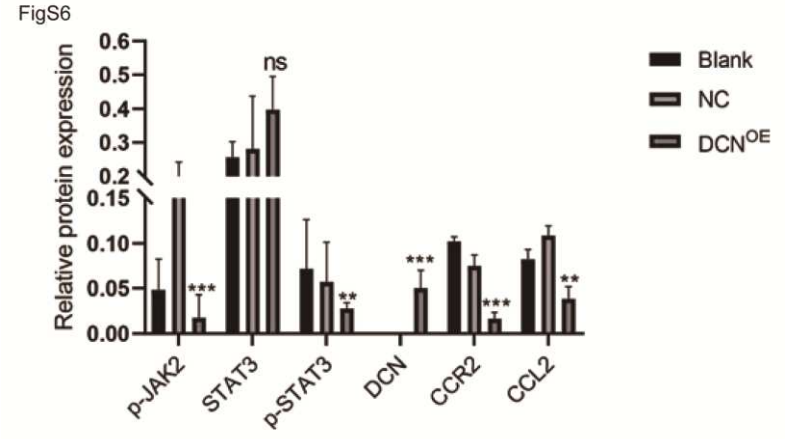
FigS4. qPCR was used to detect DCN expression in THP-1 cells transfected with lentivirus; "***" indicates P < 0.001.

FigS5



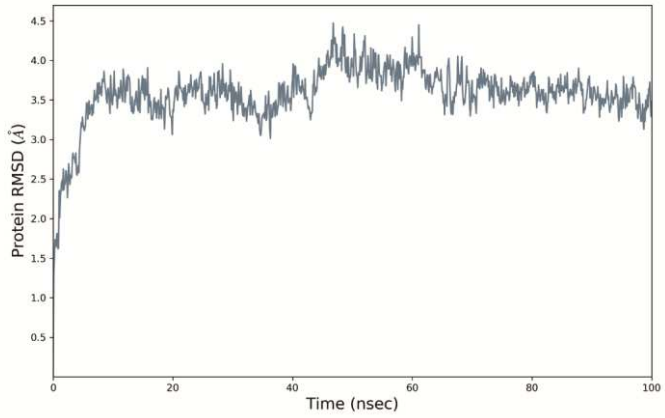
FigS5. Changes in apoptosis of colorectal cancer cells co-cultured with TAMs overexpressing DCN.

FigS6



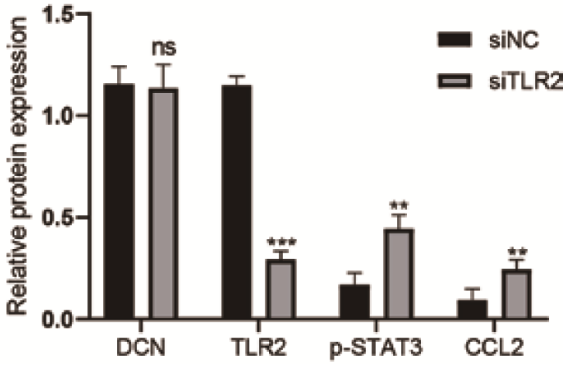
FigS6. Statistical analysis of Changes in JAK/STAT3 phosphorylation levels and CCL2/CCR2 protein levels in DCN-overexpressing TAM "*" indicates P < 0.05, "**" indicates P < 0.01, and "***" indicates P < 0.001.

FigS7

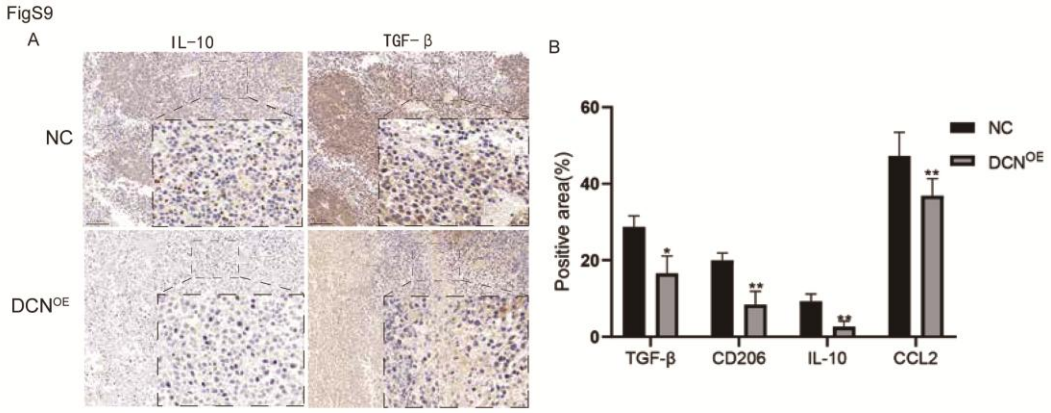


FigS7. Analysis of the interaction mechanism between DCN and TLR2.

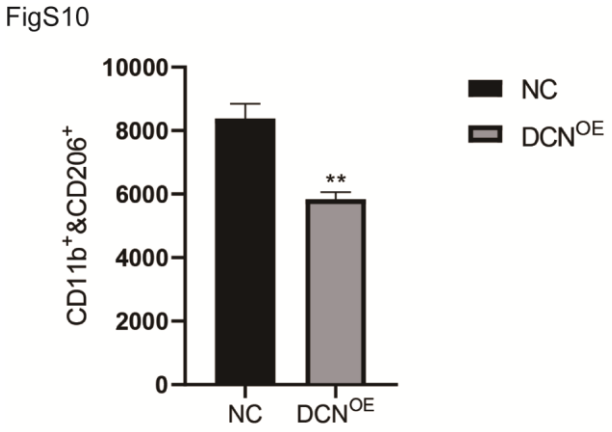
FigS8



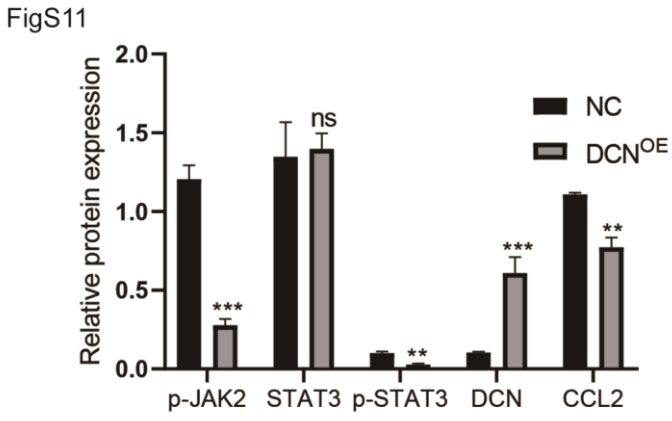
FigS8. Statistical analysis of western blot analysis detecting changes in STAT3 phosphorylation levels and CCL2 protein levels following TLR2 knockout; "*" indicates P < 0.05, "**" indicates P < 0.01, and "***" indicates P < 0.001.



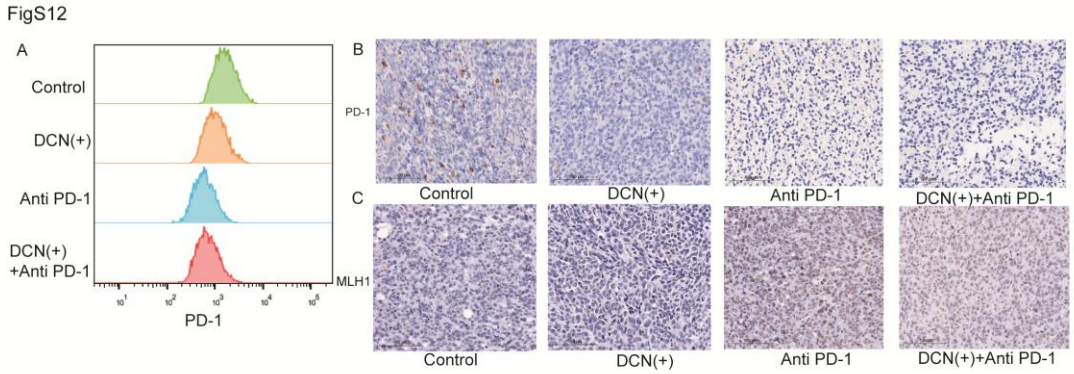
FigS9.A. Changes in tissue-resident M2-type TAM markers following DCN lentivirus treatment; B. Statistical analysis; "*" indicates P < 0.05, "**" indicates P < 0.01, and "***" indicates P < 0.001.



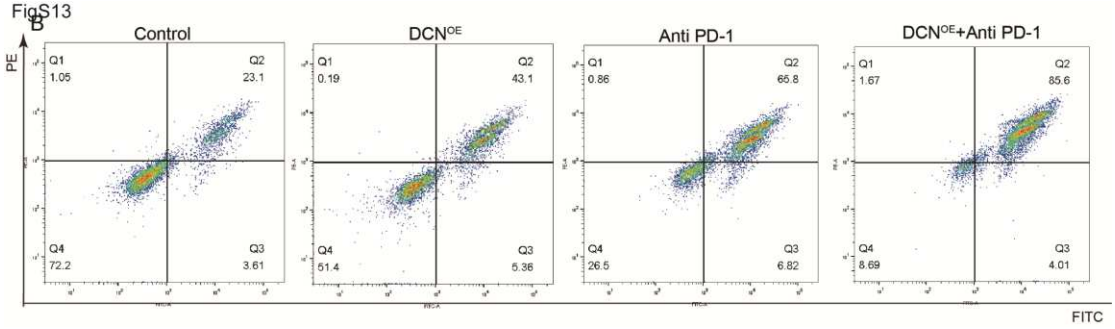
FigS10. Statistical analysis of changes in the proportion of M2-type TAMs following DCN lentivirus treatment. "*" indicates P < 0.05, "**" indicates P < 0.01, and "***" indicates P < 0.001.



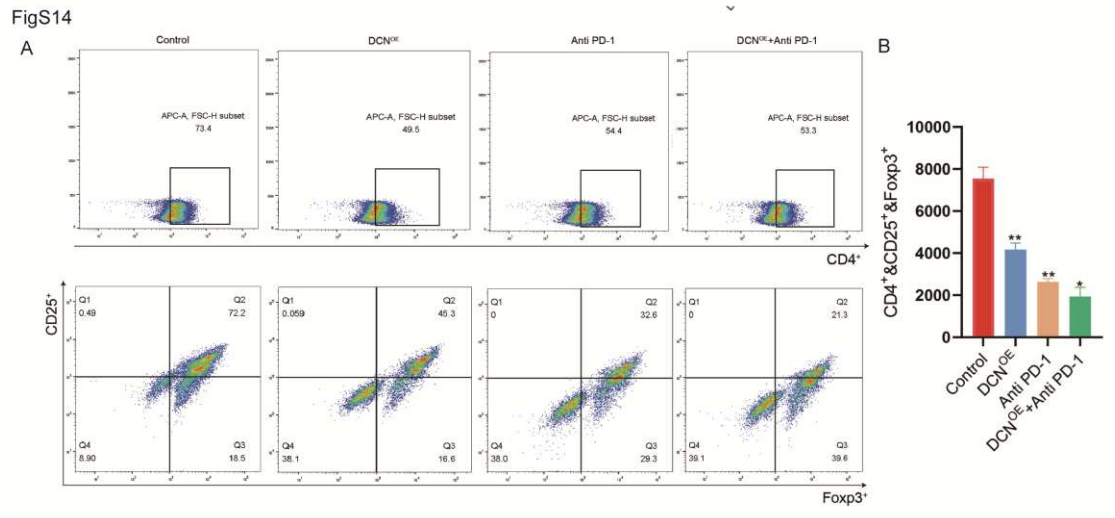
FigS11. Statistical analysis of western blot was used to detect changes in the expression of DCN, CCL2, and the JAK2-STAT3 signaling pathway in mouse M2-type TAMs; "*" indicates P < 0.05, "**" indicates P < 0.01, and "***" indicates P < 0.001.



FigS12. A. Flow cytometry was used to detect the effect of PD-1 immune checkpoint inhibitors on TAMs in mouse tumor tissue; B. Immunohistochemistry was used to detect the expression of PD-1 in tissues after treatment with PD-1 immune checkpoint inhibitors ;C. Immunohistochemistry was used to detect the expression of MLH1 in tissues after treatment with PD-1 immune checkpoint inhibitors.



FigS13. Flow cytometry was used to detect the effect of combined treatment with PD-1 immune checkpoint inhibitors and DCN lentiviral vector on apoptosis of mouse tumor cells.



FigS14. Flow cytometry analysis of changes in Treg cell proportion after combined treatment with DCN lentivirus and PD-1 immune checkpoint inhibitor; "*" indicates $P < 0.05$, "**" indicates $P < 0.01$, and "***" indicates $P < 0.001$.

Reference

1 Primm, K. M., Blackman, E., Sansbury, B. M., Zaidi, S. K. & Sengupta, R. AACR Pediatric Cancer Progress Report 2025. *Clin Cancer Res* **32**, 465-467, doi:10.1158/1078-0432.Ccr-25-4722 (2026).

2 Li, Q. *et al.* Signaling pathways involved in colorectal cancer: pathogenesis and targeted therapy. *Signal Transduct Target Ther* **9**, 266, doi:10.1038/s41392-024-01953-7 (2024).

3 Leiphrakpam, P. D. & Are, C. PI3K/Akt/mTOR Signaling Pathway as a Target for Colorectal Cancer Treatment. *Int J Mol Sci* **25**, doi:10.3390/ijms25063178 (2024).

4 Genova, C. *et al.* Therapeutic Implications of Tumor Microenvironment in Lung Cancer: Focus on Immune Checkpoint Blockade. *Front Immunol* **12**, 799455, doi:10.3389/fimmu.2021.799455 (2021).

5 Li, J. *et al.* Remodeling of the immune and stromal cell compartment by PD-1 blockade in mismatch repair-deficient colorectal cancer. *Cancer Cell* **41**, 1152-1169 e1157, doi:10.1016/j.ccell.2023.04.011 (2023).

6 Mei, W. J. *et al.* Clinicopathological characteristics of high microsatellite instability/mismatch repair-deficient colorectal cancer: A narrative review. *Front Immunol* **13**, 1019582, doi:10.3389/fimmu.2022.1019582 (2022).

7 Lin, A., Zhang, J. & Luo, P. Crosstalk Between the MSI Status and Tumor Microenvironment in Colorectal Cancer. *Front Immunol* **11**, 2039, doi:10.3389/fimmu.2020.02039 (2020).

8 Wang, F. *et al.* Single-cell and spatial transcriptome analysis reveals the cellular heterogeneity of liver metastatic colorectal cancer. *Science advances* **9**, eadf5464, doi:10.1126/sciadv.adf5464 (2023).

9 Valdeolivas, A. *et al.* Profiling the heterogeneity of colorectal cancer consensus molecular subtypes using spatial transcriptomics. *NPJ Precis Oncol* **8**, 10, doi:10.1038/s41698-023-00488-4 (2024).

10 Planque, M., Igelmann, S., Ferreira Campos, A. M. & Fendt, S. M. Spatial metabolomics principles and application to cancer research. *Curr Opin Chem Biol* **76**, 102362, doi:10.1016/j.cbpa.2023.102362 (2023).

11 Gao, J., Liang, Y. & Wang, L. Shaping Polarization Of Tumor-Associated Macrophages In Cancer Immunotherapy. *Front Immunol* **13**, 888713, doi:10.3389/fimmu.2022.888713 (2022).

12 Yang, M., Li, J., Gu, P. & Fan, X. The application of nanoparticles in cancer immunotherapy: Targeting tumor microenvironment. *Bioactive Materials* **6**, 1973-1987, doi:10.1016/j.bioactmat.2020.12.010 (2021).

13 Nicolini, A. & Ferrari, P. Involvement of tumor immune microenvironment metabolic reprogramming in colorectal cancer progression, immune escape, and response to immunotherapy. *Front Immunol* **15**, 1353787, doi:10.3389/fimmu.2024.1353787 (2024).

14 Geltz, A., Geltz, J. & Kasprzak, A. Regulation and Function of Tumor-Associated Macrophages (TAMs) in Colorectal Cancer (CRC): The Role of the SRIF System in Macrophage Regulation. *Int J Mol Sci* **26**, doi:10.3390/ijms26115336 (2025).

15 Zhao, M. *et al.* Targeting MAPK14 by Lobeline Upregulates Slurp1-Mediated Inhibition

of Alternative Activation of TAM and Retards Colorectal Cancer Growth. *Adv Sci (Weinh)* **12**, e2407900, doi:10.1002/advs.202407900 (2025).

16 Wang, X. *et al.* HMGA2 facilitates colorectal cancer progression via STAT3-mediated tumor-associated macrophage recruitment. *Theranostics* **12**, 963-975, doi:10.7150/thno.65411 (2022).

17 Singh, S., Anshita, D. & Ravichandiran, V. MCP-1: Function, regulation, and involvement in disease. *Int Immunopharmacol* **101**, 107598, doi:10.1016/j.intimp.2021.107598 (2021).

18 Wei, X. *et al.* Disruption of tumor-intrinsic PGAM5 increases anti-PD-1 efficacy through the CCL2 signaling pathway. *J Immunother Cancer* **13**, doi:10.1136/jitc-2024-009993 (2025).

19 Chen, X. *et al.* PIM1/NF-κB/CCL2 blockade enhances anti-PD-1 therapy response by modulating macrophage infiltration and polarization in tumor microenvironment of NSCLC. *Oncogene* **43**, 2517-2530, doi:10.1038/s41388-024-03100-6 (2024).

20 Yamada, K. *et al.* E7386, a Selective Inhibitor of the Interaction between β-Catenin and CBP, Exerts Antitumor Activity in Tumor Models with Activated Canonical Wnt Signaling. *Cancer Res* **81**, 1052-1062, doi:10.1158/0008-5472.Can-20-0782 (2021).

21 Zhao, H. *et al.* Oncolytic Adenovirus rAd.DCN Inhibits Breast Tumor Growth and Lung Metastasis in an Immune-Competent Orthotopic Xenograft Model. *Hum Gene Ther* **30**, 197-210, doi:10.1089/hum.2018.055 (2019).

22 Soria-Valles, C. *et al.* Correction: The anti-metastatic activity of collagenase-2 in breast cancer cells is mediated by a signaling pathway involving decorin and miR-21. *Oncogene* **38**, 5739, doi:10.1038/s41388-019-0825-3 (2019).

23 Sainio, A. O. & Järveläinen, H. T. Decorin-mediated oncosuppression - a potential future adjuvant therapy for human epithelial cancers. *British journal of pharmacology* **176**, 5-15, doi:10.1111/bph.14180 (2019).

24 Appunni, S. *et al.* Decorin: matrix-based pan-cancer tumor suppressor. *Molecular and cellular biochemistry* **480**, 3569-3591, doi:10.1007/s11010-025-05224-z (2025).

25 Cui, J. *et al.* Decorin attenuates hypertrophic scar fibrosis via TGFβ/Smad signalling. *Experimental dermatology* **33**, e15133, doi:10.1111/exd.15133 (2024).

26 Merline, R. *et al.* Signaling by the matrix proteoglycan decorin controls inflammation and cancer through PDCD4 and MicroRNA-21. *Science signaling* **4**, ra75, doi:10.1126/scisignal.2001868 (2011).

27 Kim, K. T. *et al.* Decorin as a key marker of desmoplastic cancer-associated fibroblasts mediating first-line immune checkpoint blockade resistance in metastatic gastric cancer. *Gastric cancer : official journal of the International Gastric Cancer Association and the Japanese Gastric Cancer Association* **28**, 12-26, doi:10.1007/s10120-024-01567-6 (2025).

28 Buraschi, S., Neill, T. & Iozzo, R. V. Decorin is a devouring proteoglycan: Remodeling of intracellular catabolism via autophagy and mitophagy. *Matrix Biol* **75-76**, 260-270, doi:10.1016/j.matbio.2017.10.005 (2019).

29 Mao, L. *et al.* Decorin deficiency promotes epithelial-mesenchymal transition and colon cancer metastasis. *Matrix Biol* **95**, 1-14, doi:10.1016/j.matbio.2020.10.001 (2021).

30 Mondal, D. K., Xie, C., Pascal, G. J., Buraschi, S. & Iozzo, R. V. Decorin suppresses tumor lymphangiogenesis: A mechanism to curtail cancer progression. *Proc Natl Acad Sci U S*

A **121**, e2317760121, doi:10.1073/pnas.2317760121 (2024).
31 Bi, X. L. & Yang, W. Biological functions of decorin in cancer. *Chinese journal of cancer* **32**, 266-269, doi:10.5732/cjc.012.10301 (2013).
32 Liu, J. *et al.* DCN released from ferroptotic cells ignites AGER-dependent immune responses. *Autophagy* **18**, 2036-2049, doi:10.1080/15548627.2021.2008692 (2022).
33 Bi, X. *et al.* Oncogenic activin C interacts with decorin in colorectal cancer in vivo and in vitro. *Mol Carcinog* **55**, 1786-1795, doi:10.1002/mc.22427 (2016).
34 Fujiwara, T. *et al.* Role of Tumor-Associated Macrophages in Sarcomas. *Cancers (Basel)* **13**, doi:10.3390/cancers13051086 (2021).
35 Hogg, S. J. *et al.* Distinct modulation of IFN γ -induced transcription by BET bromodomain and catalytic P300/CBP inhibition in breast cancer. *Clinical epigenetics* **14**, 96, doi:10.1186/s13148-022-01316-5 (2022).
36 Osna, N. A., Rasineni, K., Ganesan, M., Donohue, T. M., Jr. & Kharbanda, K. K. Pathogenesis of Alcohol-Associated Liver Disease. *Journal of clinical and experimental hepatology* **12**, 1492-1513, doi:10.1016/j.jceh.2022.05.004 (2022).
37 Kerzel, T. *et al.* In vivo macrophage engineering reshapes the tumor microenvironment leading to eradication of liver metastases. *Cancer Cell* **41**, 1892-1910.e1810, doi:10.1016/j.ccell.2023.09.014 (2023).
38 Xu, M., Wang, Y., Xia, R., Wei, Y. & Wei, X. Role of the CCL2-CCR2 signalling axis in cancer: Mechanisms and therapeutic targeting. *Cell Prolif* **54**, e13115, doi:10.1111/cpr.13115 (2021).
39 Korbecki, J. *et al.* CC Chemokines in a Tumor: A Review of Pro-Cancer and Anti-Cancer Properties of the Ligands of Receptors CCR1, CCR2, CCR3, and CCR4. *Int J Mol Sci* **21**, doi:10.3390/ijms21218412 (2020).
40 Kadomoto, S., Izumi, K. & Mizokami, A. Roles of CCL2-CCR2 Axis in the Tumor Microenvironment. *Int J Mol Sci* **22**, doi:10.3390/ijms22168530 (2021).
41 Zhao, L. *et al.* LINC00330/CCL2 axis-mediated ESCC TAM reprogramming affects tumor progression. *Cell Mol Biol Lett* **29**, 77, doi:10.1186/s11658-024-00592-8 (2024).
42 Xu, J. *et al.* Dual roles and therapeutic targeting of tumor-associated macrophages in tumor microenvironments. *Signal Transduct Target Ther* **10**, 268, doi:10.1038/s41392-025-02325-5 (2025).
43 Chen, X. *et al.* CCL2-targeted ginkgolic acid exerts anti-glioblastoma effects by inhibiting the JAK3-STAT1/PI3K-AKT signaling pathway. *Life sciences* **311**, 121174, doi:10.1016/j.lfs.2022.121174 (2022).
44 Hao, Q., Vadgama, J. V. & Wang, P. CCL2/CCR2 signaling in cancer pathogenesis. *Cell Commun Signal* **18**, 82, doi:10.1186/s12964-020-00589-8 (2020).
45 Pozzi, S. & Satchi-Fainaro, R. The role of CCL2/CCR2 axis in cancer and inflammation: The next frontier in nanomedicine. *Adv Drug Deliv Rev* **209**, 115318, doi:10.1016/j.addr.2024.115318 (2024).
46 Sun, K. *et al.* Elevated protein lactylation promotes immunosuppressive microenvironment and therapeutic resistance in pancreatic ductal adenocarcinoma. *J Clin Invest* **135**, doi:10.1172/JCI187024 (2025).
47 Keivany, M. R., Shojae Asrami, E., Besharatloo, M., Latifi, H. & Barjasteh, A. H. Advances in immunotherapy for colorectal cancer: overcoming resistance in mismatch repair-

proficient tumors. *Cancer Cell Int* **26**, doi:10.1186/s12935-026-04177-7 (2026).

48 Yousefi, M., Amirabadi, D. G., Javan, M. R. & Khosrojerdi, A. Immune escape in colorectal cancer: Mechanisms and challenges of immune checkpoint inhibitor resistance. *Int Immunopharmacol* **169**, 115986, doi:10.1016/j.intimp.2025.115986 (2026).

49 Lin, K. X. *et al.* PD-1 and PD-L1 inhibitors in cold colorectal cancer: challenges and strategies. *Cancer Immunol Immunother* **72**, 3875-3893, doi:10.1007/s00262-023-03520-5 (2023).

50 Lin, H. *et al.* LRP1 induces anti-PD-1 resistance by modulating the DLL4-NOTCH2-CCL2 axis and redirecting M2-like macrophage polarisation in bladder cancer. *Cancer Lett* **593**, 216807, doi:10.1016/j.canlet.2024.216807 (2024).

51 Yang, H. *et al.* CCL2-CCR2 axis recruits tumor associated macrophages to induce immune evasion through PD-1 signaling in esophageal carcinogenesis. *Mol Cancer* **19**, 41, doi:10.1186/s12943-020-01165-x (2020).

52 Israeli Dangoor, S. *et al.* CCL2 blockade combined with PD-1/P-selectin immunomodulators impedes breast cancer brain metastasis. *Brain* **148**, 1740-1756, doi:10.1093/brain/awae347 (2025).

Supplementary Files

This is a list of supplementary files associated with this preprint. Click to download.

- supplementarymaterials.docx